The Abdus Salam
International Centre for Theoretical Physics

United Nations
Educational, Scientific
and Cultural Organization

International Atomic
Energy Agency

World Year of
PHYSICS
2005

SMR.1670 - 24

INTRODUCTION TO MICROFLUIDICS

8 - 26 August 2005

Mixing in Micro-Flows

V. Steinberg
Weizmann Institute of Science, Israel

Strada Costiera 11, 34014 Trieste, Italy - Tel. +39 040 2240 111; Fax +39 040 224 163 - sci_info@ictp.it, www.ictp.it

Mixing in micro-flows

(Various approaches to the same problem:
Enhancement of mixing)

V. Steinberg

Lecture 4

**Summer School in Microfluidics,
August 8-26, 2005, ICTP, Trieste, Italy**

WEIZMANN
INSTITUTE
OF SCIENCE

Methods used up to now:

1. 3D serpentine to promote chaotic mixing (Re>1)
2. 3D micro-vascular network
3. Placement of slanted walls at T-junctions
4. Flow obstacles
5. Electro-kinetic flow instability
6. Electro-hydrodynamic mixing
7. Hydrodynamic focusing
8. Internal circulation in droplets under shear
9. Bas-relief structures on the walls or floor of the channel to initiate steady chaotic mixing (staggering herringbone mixer)
10. Topological mixing (Hamiltonian chaos)
11. Periodic chaotic flow (spatio-temporal resonances)
12. Complex visco-elastic flow

mostly passive mixers will be discussed

Elastic flow instability, curved streamlines, and mixing in microfluidic flows

Jai A. Pathak
National Institute of Standards and Technology, Polymers Division, Gaithersburg, Maryland 20899-8544

David Ross
National Institute of Standards and Technology, Process Measurements Division, Gaithersburg, Maryland 20899-8362

Kalman B. Migler
National Institute of Standards and Technology, Polymers Division, Gaithersburg, Maryland 20899-8544

Polymer solution-elasticity+streamline curvature lead to elastic flow instability

Zig-zag channel in polycarbonate
85x60 microns, 50 elements

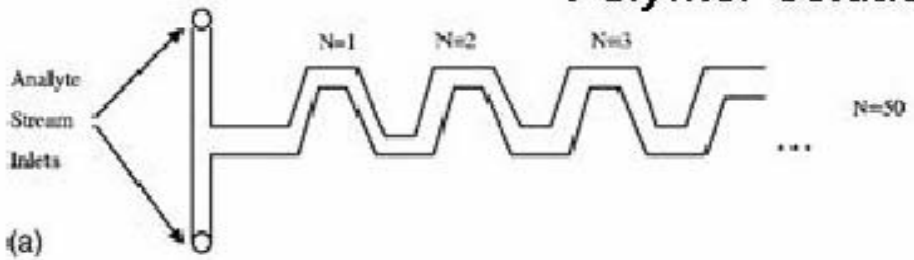

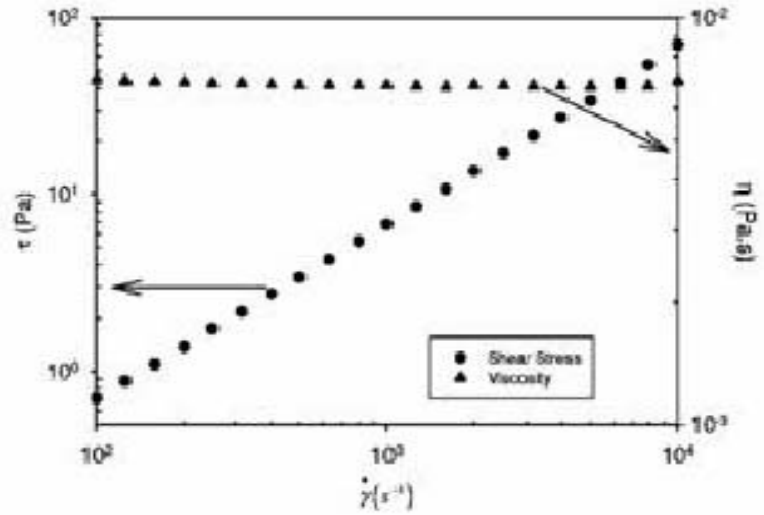

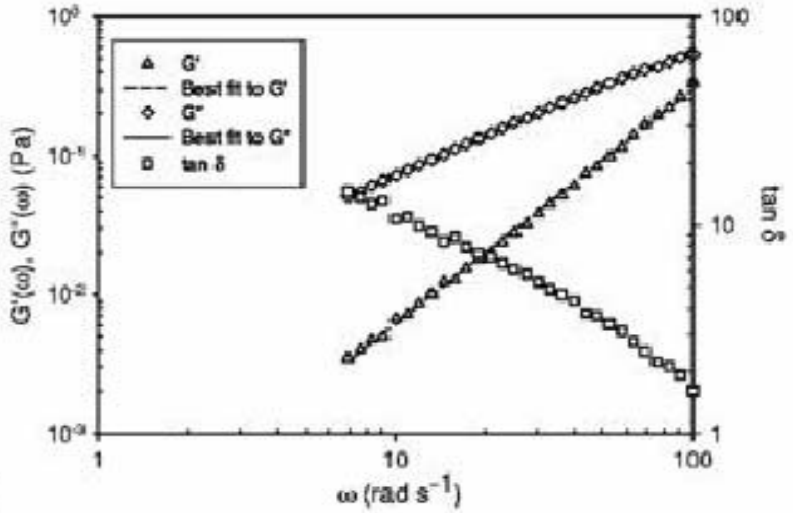

66 ppm PAAm (18MDa), low viscosity (6.8 of water)

Quantification of mixing

$$D_i = \left[\frac{1}{N} \sum_{i=1}^{N} (I_i - I_{\max})^2 \right]^{1/2}$$

-deviation from mixing that is normalized by the value at the incoming junction

I_i and $I_{\max}$ are the intensity at pixel I and the maximum intensity, respectively, observed at any pixel in a fully mixed system

N is the number of pixels

$D_{i,norm}$ has value 0 for perfectly mixed state, and value 1 for completely unmixed one

$t_{res} \propto Q^{-1}$ for Newtonian fluid where **Q** is the fluid discharge

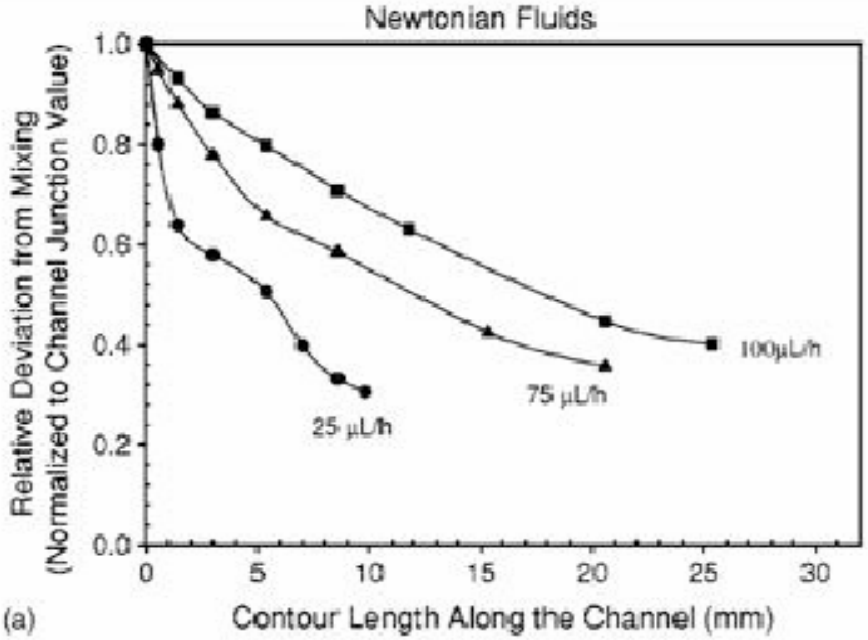

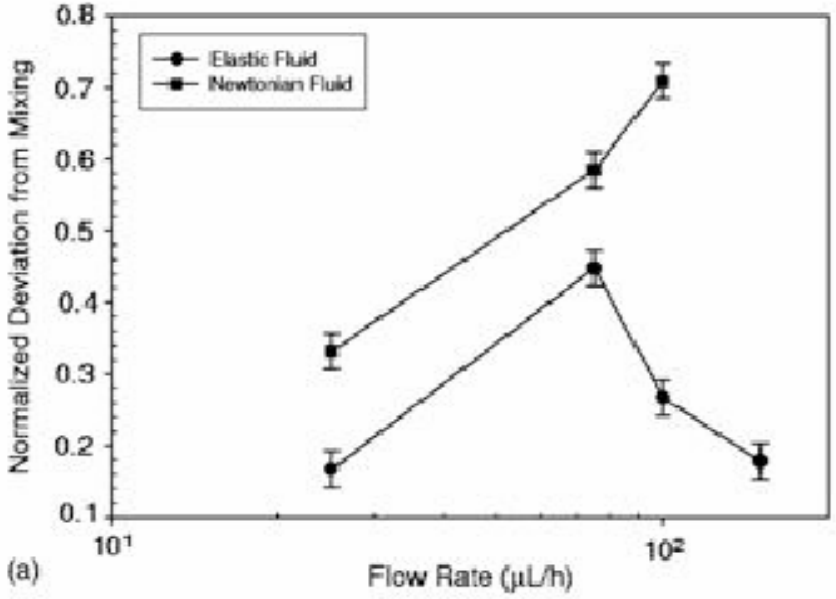

$$0 \le D_i \le 1$$ 1-unmixed,0-perfectly mixed

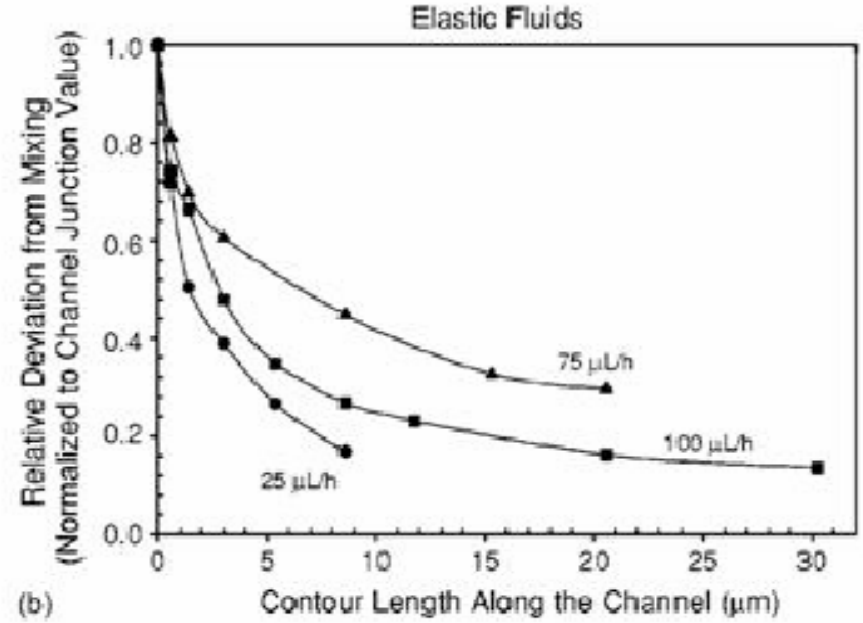

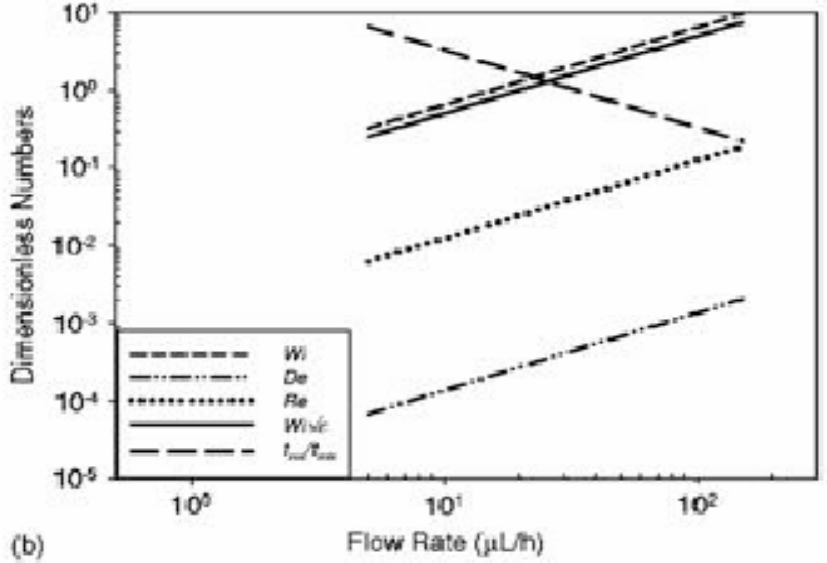

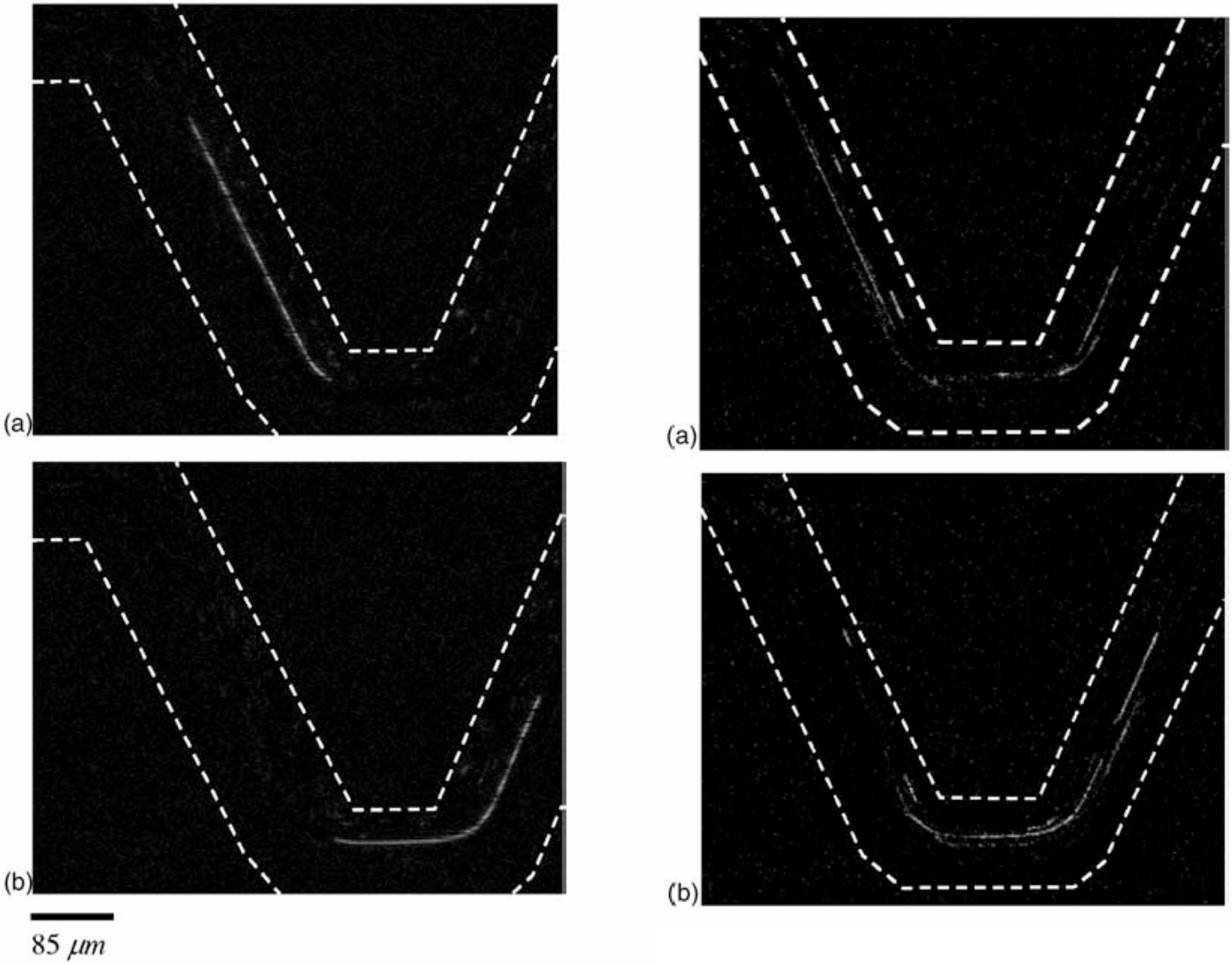
(a)
(b)
85 μm
(a)
(b)

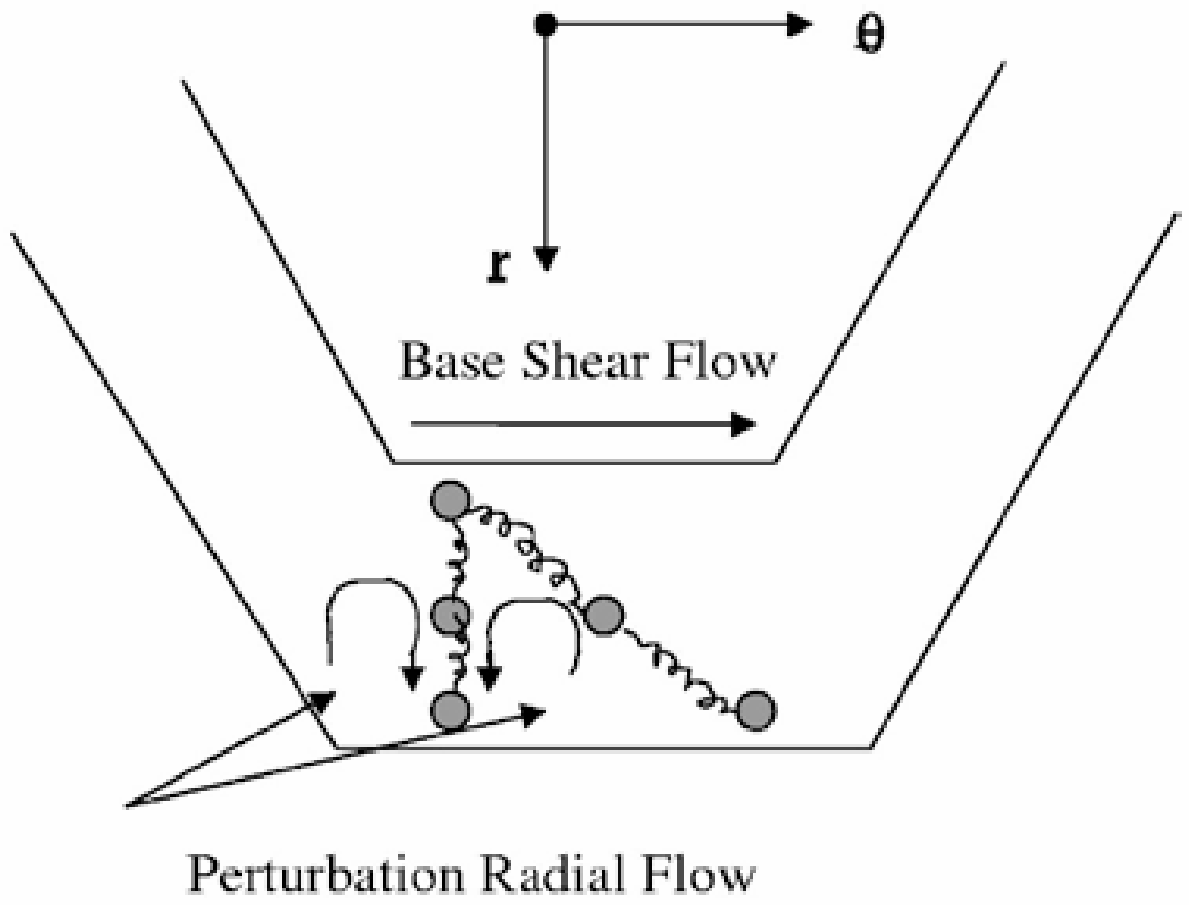

FIG. 6. Schematic of the axisymmetric mode of the instability in the flow of the elastic fluid in the Taylor–Couette setup (adapted from Ref. 36).

Parameters of the experiment and characterization of mixing effectiveness

- Solution low viscosity results in rather high velocity at the elastic instability threshold and rather small

$$t_{res} = L / \langle V \rangle$$

- Rather high diffusion coefficient of fluorescent dye leads to effective diffusive mixing ($D = 10^{-6} cm^2 / s$)

- Geometry of the micro-channel and flow regime result in rather low effective mixing compared with elastic turbulence (2-3 times instead of 5-6 orders)

- Due to poor characterization of the flow (velocity and concentration fields) it is not clear what is the character of the flow

Staggered herringbone mixer (SHM)

A. Stroock et al, Science 295, 647 (2002)

- Relevant parameters of the problem:

$$\mathrm{Re} = Vl/\nu \geq 1 \qquad Pe = Vl/D >> 1$$

- Mixing length along the channel:

$$l_{mix} \propto V \times (l^2/D) = Pe \times l$$

can be extremely long and grows *linearly* with Pe

- Solution for the problem-transverse flow component that stretches and folds a fluid element and in this way reduces the mixing length by decreasing the average distance over which the diffusion should act. One of the possibilities- stationary chaotic flow. Then the mixing length

$$l_{mix} \propto l \ln(Pe)$$ and ***0<Re<100***

From simple to three-dimensional laminar flows: Controlling flow with topography

Anisotropic Response: More resistance to flow over bumps (x) than along ridges and valleys (*y*) (transverse response)
Corrugations produce a three-dimensional flow!
This kind of effect is very useful for mixing!

Ridges produce anisotropic resistance to viscous flow and generate helical circulation flow

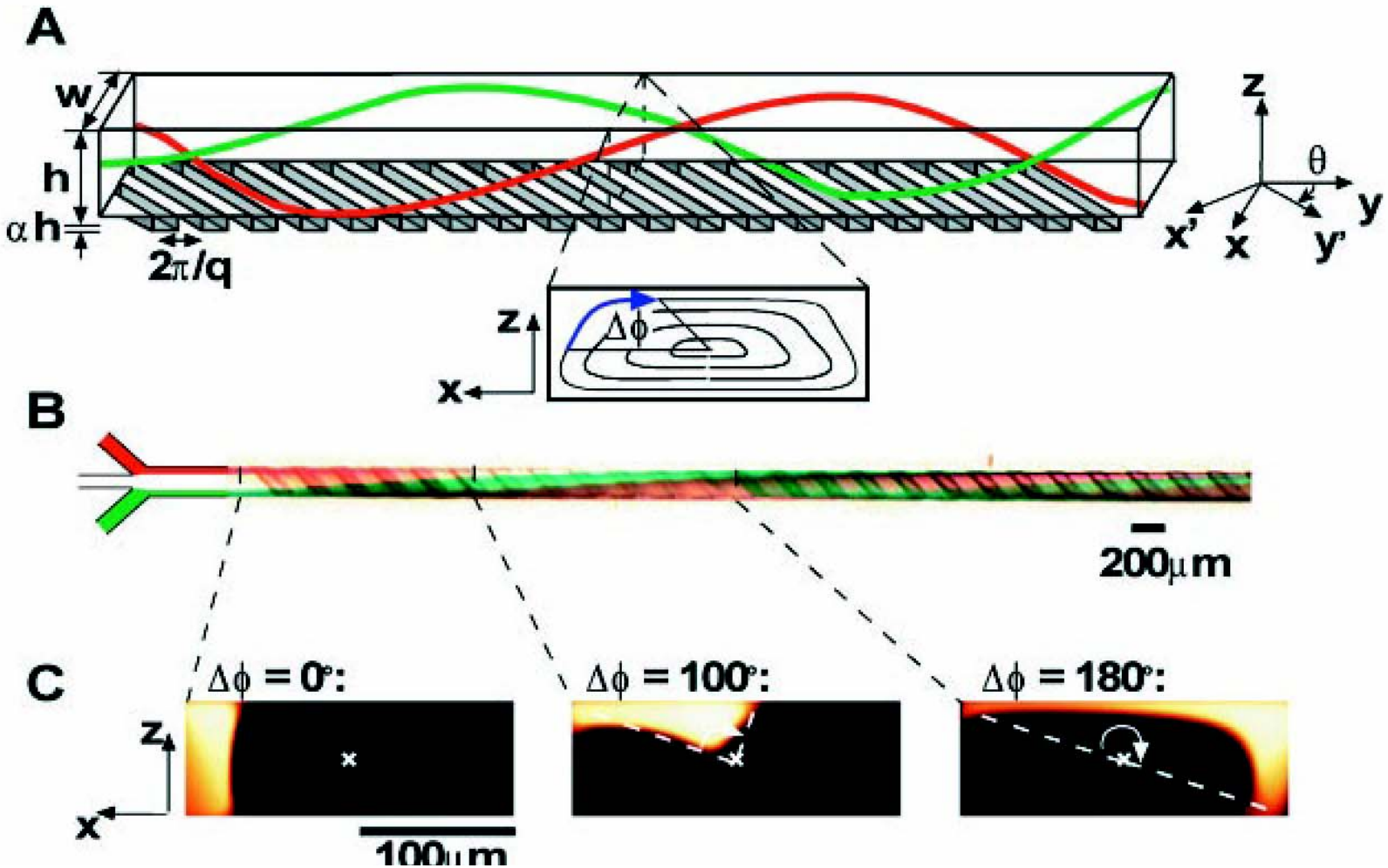

Confocal micrographs

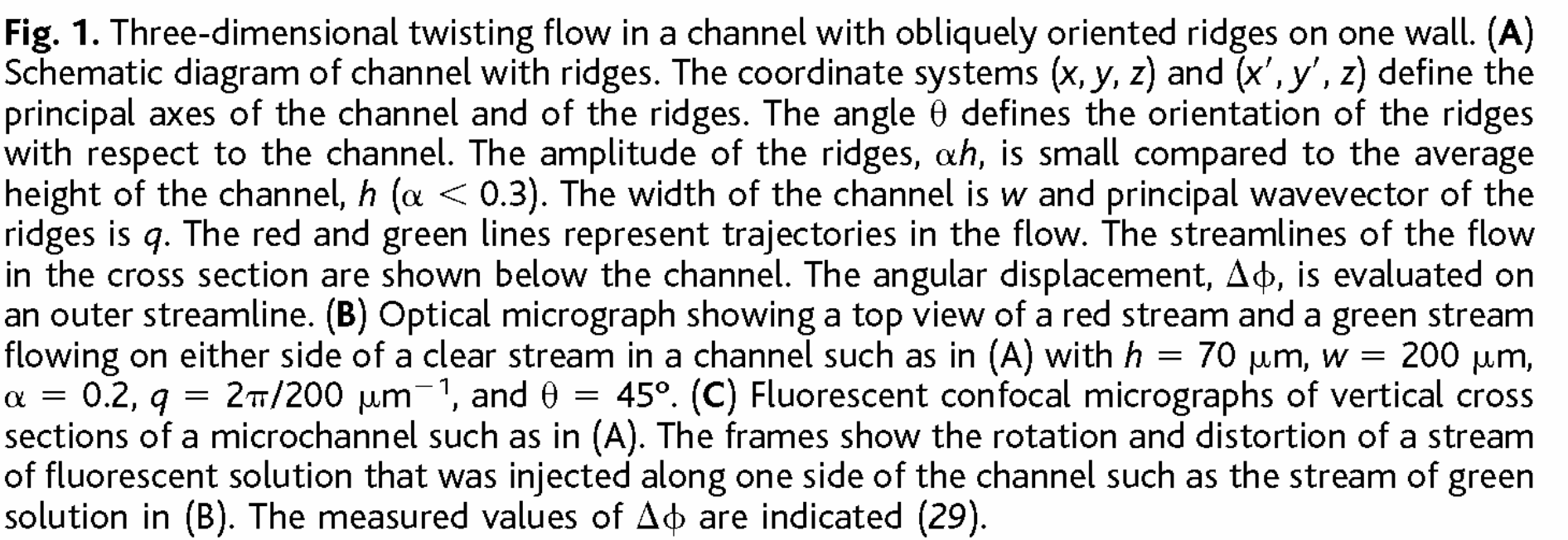

Fig. 1. Three-dimensional twisting flow in a channel with obliquely oriented ridges on one wall. (**A**) Schematic diagram of channel with ridges. The coordinate systems (x, y, z) and (x', y', z) define the principal axes of the channel and of the ridges. The angle θ defines the orientation of the ridges with respect to the channel. The amplitude of the ridges, αh, is small compared to the average height of the channel, h ($\alpha < 0.3$). The width of the channel is w and principal wavevector of the ridges is q. The red and green lines represent trajectories in the flow. The streamlines of the flow in the cross section are shown below the channel. The angular displacement, $\Delta\phi$, is evaluated on an outer streamline. (**B**) Optical micrograph showing a top view of a red stream and a green stream flowing on either side of a clear stream in a channel such as in (A) with $h = 70$ μm, $w = 200$ μm, $\alpha = 0.2$, $q = 2\pi/200$ μm^{-1}, and $\theta = 45°$. (**C**) Fluorescent confocal micrographs of vertical cross sections of a microchannel such as in (A). The frames show the rotation and distortion of a stream of fluorescent solution that was injected along one side of the channel such as the stream of green solution in (B). The measured values of $\Delta\phi$ are indicated (*29*).

Staggered herringbone mixer (SHM)

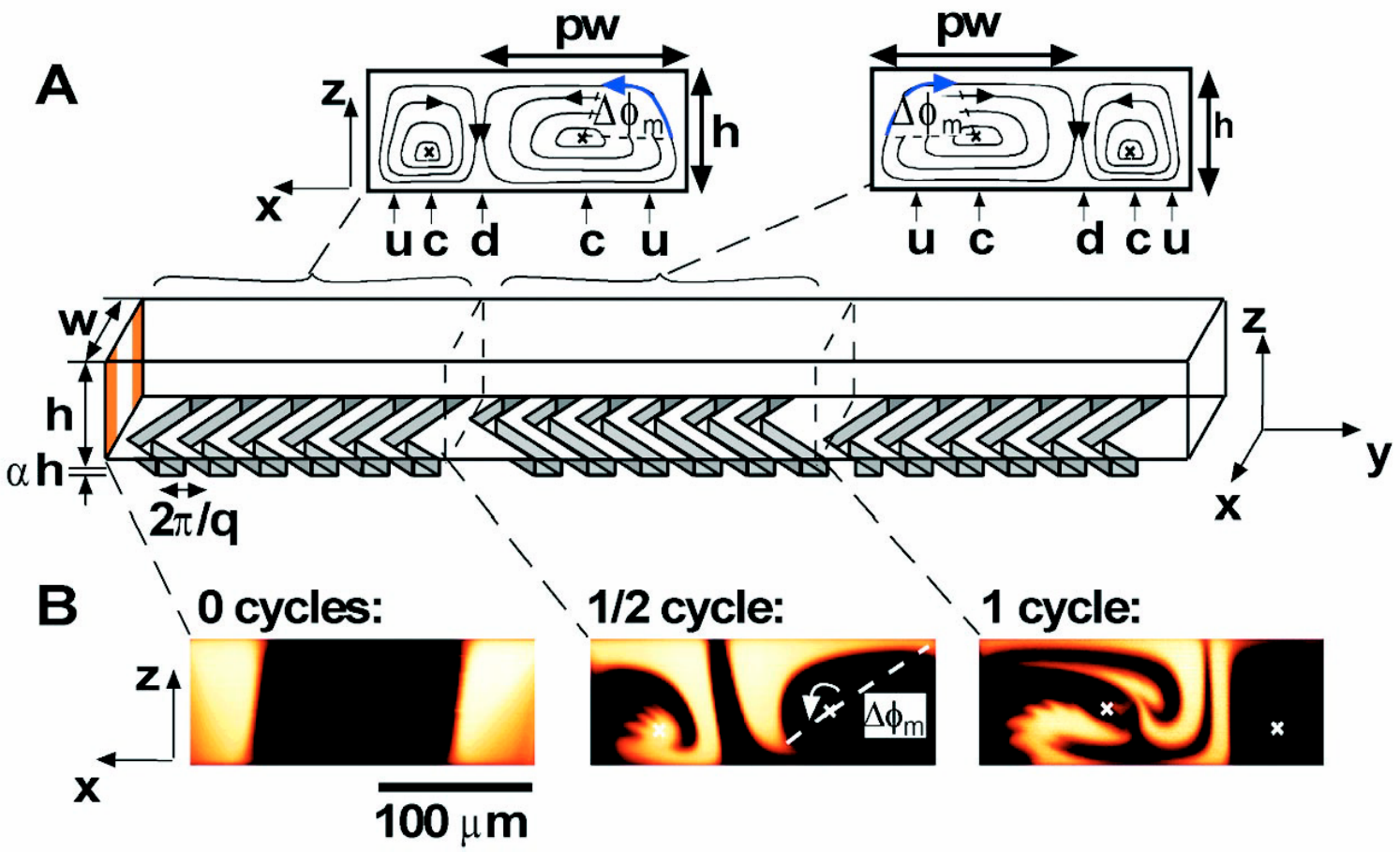

$$\mathrm{Re} < 10^{-2}$$

Fig. 2. Staggered herringbone mixer (SHM). (**A**) Schematic diagram of one-and-a-half cycles of the SHM. A mixing cycle is composed of two sequential regions of ridges; the direction of asymmetry of the herringbones switches with respect to the centerline of the channel from one region to the next. The streamlines of the flow in the cross section are shown schematically above the channel. The angle, $\Delta\phi_m$, is the average angular displacement of a volume of fluid along an outer streamline over one half cycle in the flow generated by the wide arms of the herringbones. The fraction of the width of the channel occupied by the wide arms of the herringbones is p. The horizontal positions of the centers of rotation, the upwellings, and the downwellings of the cellular flows are indicated by c, u, and d, respectively. (**B**) Confocal micrographs of vertical cross sections of a channel as in (A). Two streams of fluorescent solution were injected on either side of a stream of clear solution (*29*). The frames show the distribution of fluorescence upstream of the features, after one half cycle, and after one full cycle. The fingerlike structures at the end of the fluorescent filaments on the bottom left of the second two frames are due to the weak separation of streamlines that occurs in the rectangular grooves even at low *Re*. In this experiment, $h = 77\ \mu m$, $w = 200\ \mu m$, $\alpha = 0.23$, $q = 2\pi/100\ \mu m^{-1}$, $p = 2/3$, and $\theta = 45°$, and there were 10 ridges per half cycle. $Re < 10^{-2}$. $\Delta\phi_m \sim 180°$.

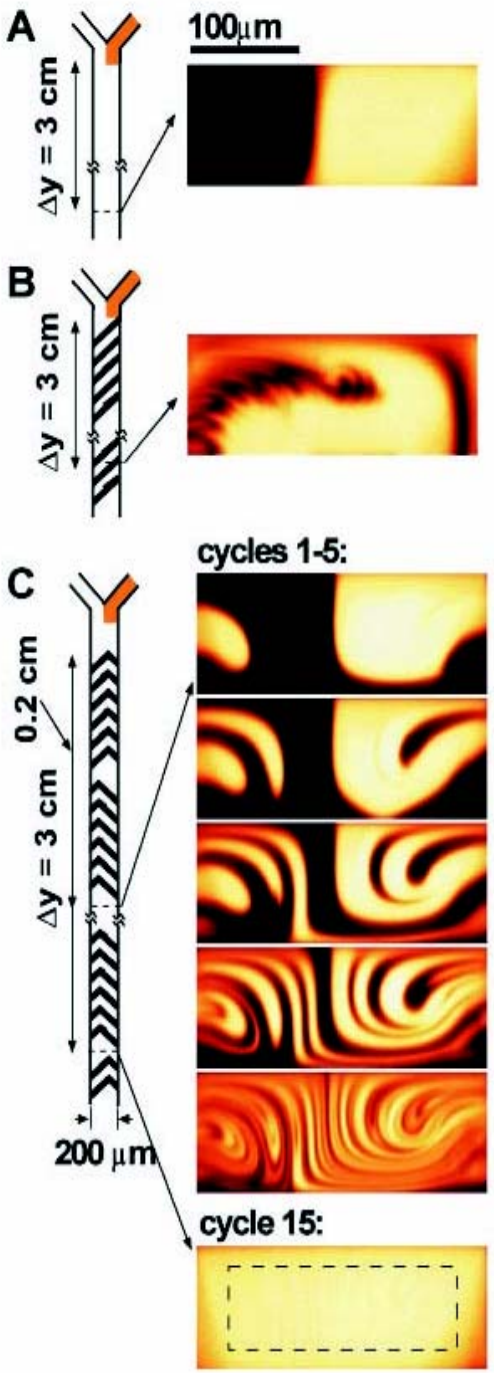

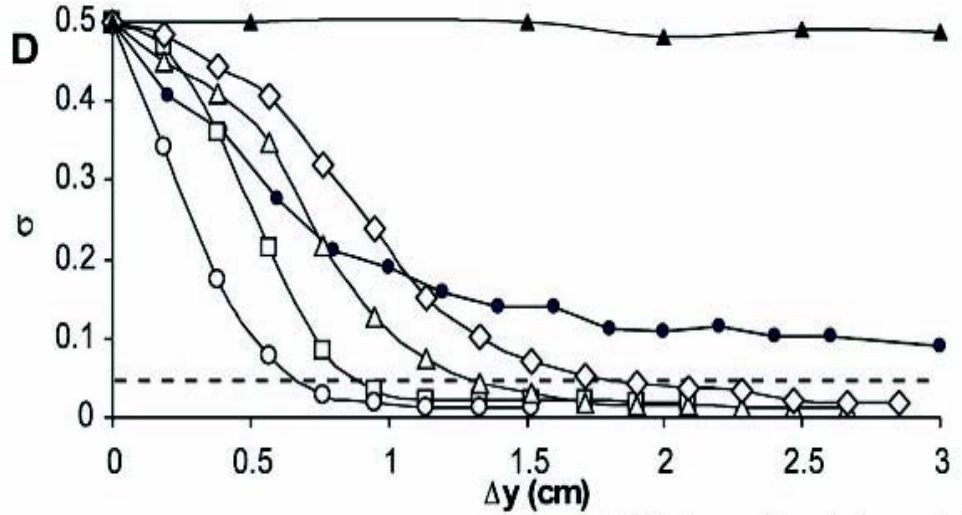

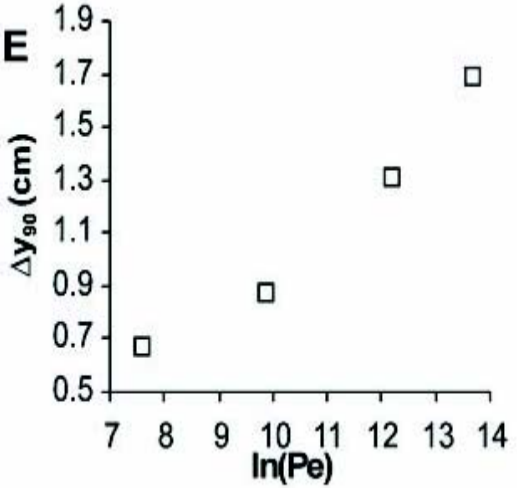

Fig. 3. Performance of SHM. (**A** to **C**) (**Left**) Schematic diagrams of channels with no structure on the walls (A), with straight ridges as in Fig. 1 (B), and with the staggered herringbone structure as in Fig. 2 (C). In each case, equal streams of a 1 mM solution of fluorescein-labeled polymer in water/glycerol mixtures (0 and 80% glycerol) and clear solution were injected into the channel (*29*, *30*). (**Right**) Confocal micrographs that show the distribution of fluorescent molecules in the cross section of the channels at a distance of 3 cm down the channels in (A) and (B) and at distances of 0.2, 0.4, 0.6, 0.8, 1.0, and 3 cm down the channel (i.e., after 1, 2, 3, 4, 5, and 15 cycles of mixing) in (C). Experimental parameters: (A) h = 70 μm, w = 200 μm, $Re \sim 10^{-2}$, $Pe = 2 \times 10^5$; (B) h = 85 μm, w = 200 μm, $\alpha = 0.18$, $\theta = 45°$, $q = 2\pi/100\ \mu m^{-1}$, $Re \sim 10^{-2}$, $Pe = 2 \times 10^5$; (C) h = 85 μm, w = 200 μm, $\alpha = 0.18$, $q = 2\pi/100\ \mu m^{-1}$, $p = 2/3$, $\theta = 45°$, $Re \sim 10^{-2}$, $Pe = 2 \times 10^5$, six ridges per half-cycle, $\Delta\phi_m \sim 60°$, $Re \sim 10^{-2}$, $Pe = 9 \times 10^5$. (**D**) Plot of the standard deviation, σ, of the fluorescence intensity in confocal images such as in (A) to (C) as a function of the distance down the channel, Δy. Only the central 50% of the area of the images [indicated in the bottom frame in (C)] was used to measure σ to eliminate variations in the fluorescence intensity due to optical effects at the channel walls. The open symbols are for the mixing channel in (C): (○) for $Pe = 2 \times 10^3$, (□) for $Pe = 2 \times 10^4$, (△) for $Pe = 2 \times 10^5$, and (◇) for $Pe = 9 \times 10^5$. $10^{-2} \leq Re \leq 10$ in these experiments. The points (▲) are for a smooth channel (A), and (●) are for a channel with straight ridges (B); for both, $Pe = 2 \times 10^5$. Horizontal dotted line indicates the value of σ used to evaluate Δy_{90}, the axial distance required for 90% mixing. (**E**) Plot of Δy_{90} as a function of ln(Pe) from the curves in (D).

Estimates of mixing length

$$D \approx 10^{-6} cm^2 / s$$

$$V = 1cm / s; l = 0.01cm$$

$$Pe = 10^4$$

$$\Delta y_m \propto Pe \times l = 100\, cm$$

$$\Delta y_{SHM} = 1cm$$

$$Pe = 10^5 \Rightarrow \Delta y_{SHM} \propto 1.5cm$$

$$\Delta y_m \propto 10^3 cm!$$

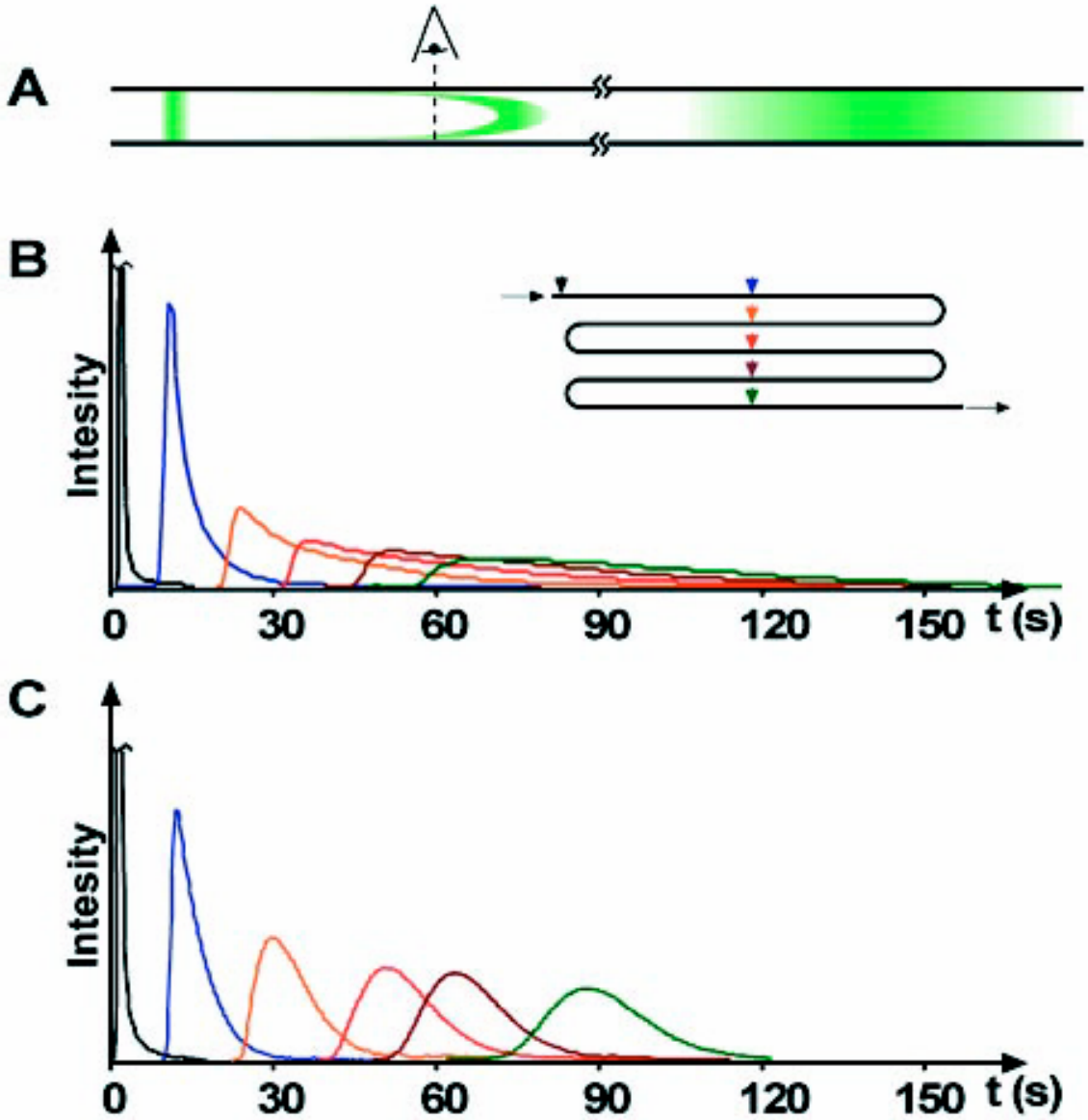

Fig. 4. Axial dispersion with and without SHM. (**A**) Schematic drawing illustrating the dispersion of a plug in Poiseuille flow. (**B**) Unstirred Poiseuille flow in a rectangular channel: $h = 70$ μm, $w = 200$ μm, and $Pe \sim 10^4$. (**C**) Stirred flow in a staggered herringbone mixer of the same design as in Fig. 3C; $Pe \sim 10^4$. In (B) and (C), a plug of fluorescent dye was introduced into serpentine channels of the form shown in the inset in (B). The traces represent the time evolution of the total fluorescence intensity (arbitrary units) as observed experimentally with a fluorescence microscope (2.5×/0.07 numerical aperture lens that averaged over the cross section of the channel) at different axial positions along the channel: 0 cm (black), 2.0 cm (blue), 6.2 cm (orange), 10.4 cm (red), 14.6 cm (brown), and 18.8 cm (green) downstream. The black traces (0 cm) have been truncated. The dye was fluorescein and the liquid was 80% glycerol/20% water. $D \sim 10^{-7}$ cm^2/s.

Topologic mixing on a microfluidic chip

Hao Chen and Jens-Christian Meiners[a)]
Department of Physics and Biophysics Research Division, University of Michigan
Ann Arbor, Michigan 48109-1120

Mixing of protein solutions due to diffusion

$$l_{mix} \equiv Pe \times l = Vl^2 / D$$

$$D = 2 \times 10^{-7} cm^2 / s$$

$$V = 0.1 cm / s; l = 0.01 cm$$

$$l_{mix} \cong 50 cm!$$

The solution for chaotic mixing: to perform series of Baker's transformations- repeated stretching and folding. As the result, the interface grows exponentially and the width of unmixed regions decreases exponentially in time

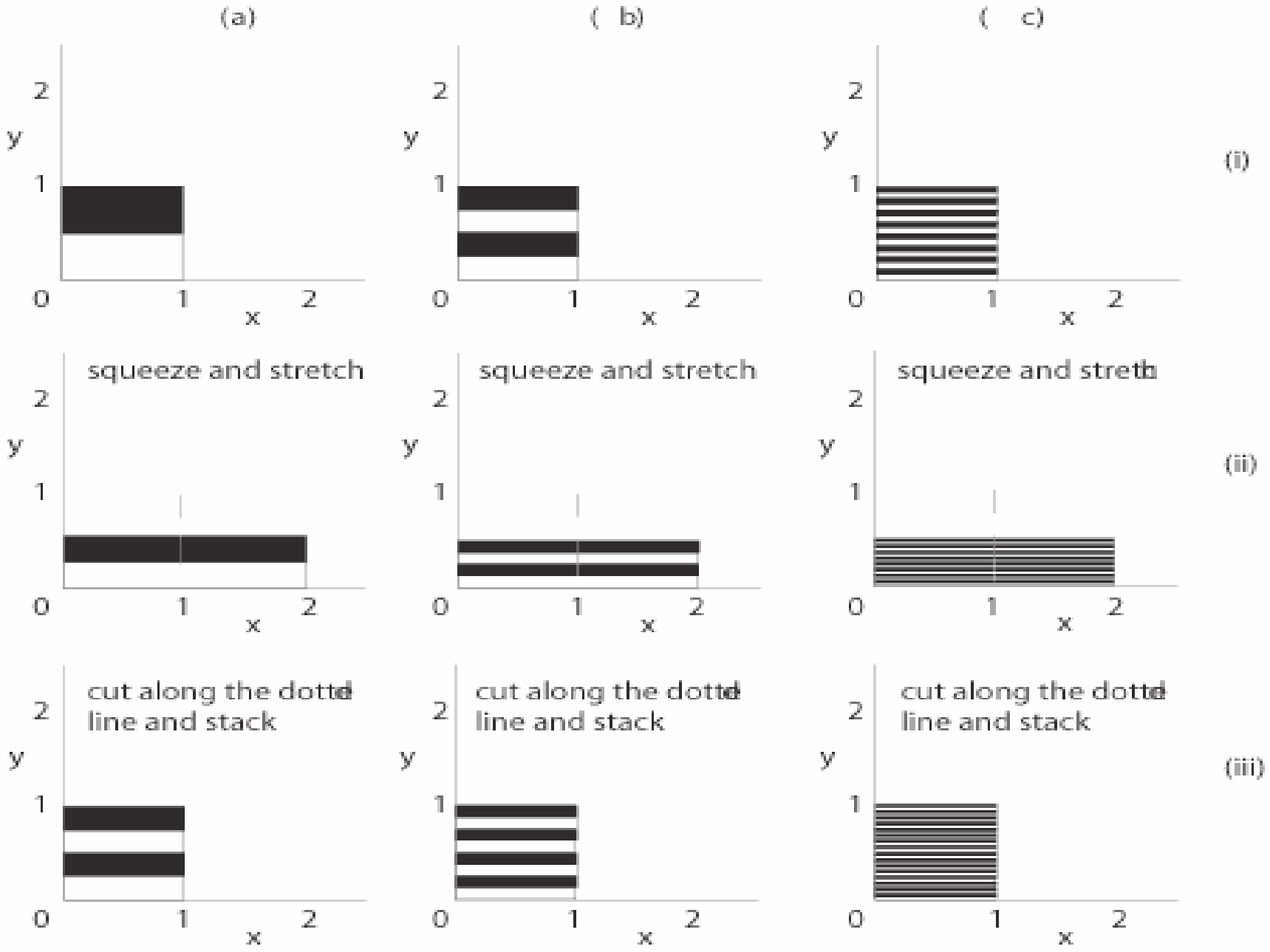

Baker's transformation

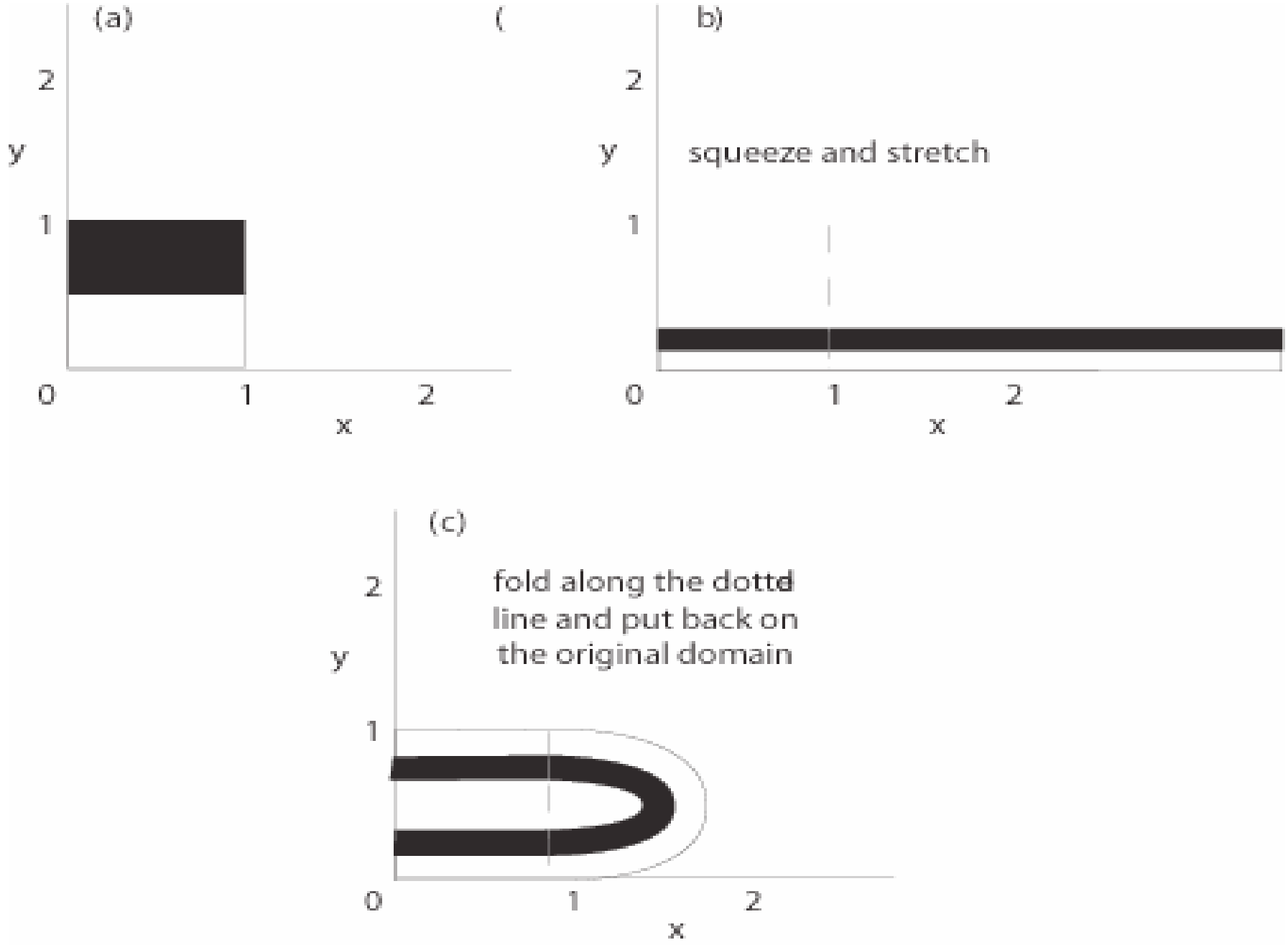

Figure 2. The Smale horseshoe map acting on the unit square.
Note the loss of material from the original domain (the unit square).

Description of principle of topological mixer

Topological mixer consists of microfluidic elements –splitters, turns, and combiners -that retain the concentration profile across the channel. Flow is splitted into two identical streams, and through series of turns, rotate the concentration profile by $\pi/2$ in opposite direction in each channel. Upon recombination, the concentration profile gradients are doubled.

Topological structure leads to repeatedly fold the flow and double the lateral concentration gradient deterministically in a very compact geometry. So, it Performs a series of Baker's transformations on the concentration profiles. This creates a layered fluid stream in a process that decreases the required channel length exponentially with the number of microfluidic elements on the chip. (It is in contrast to flow laminating technique, e.g. micro-nozzle, that only quadratically decreases the mixing length with the number of elements.)

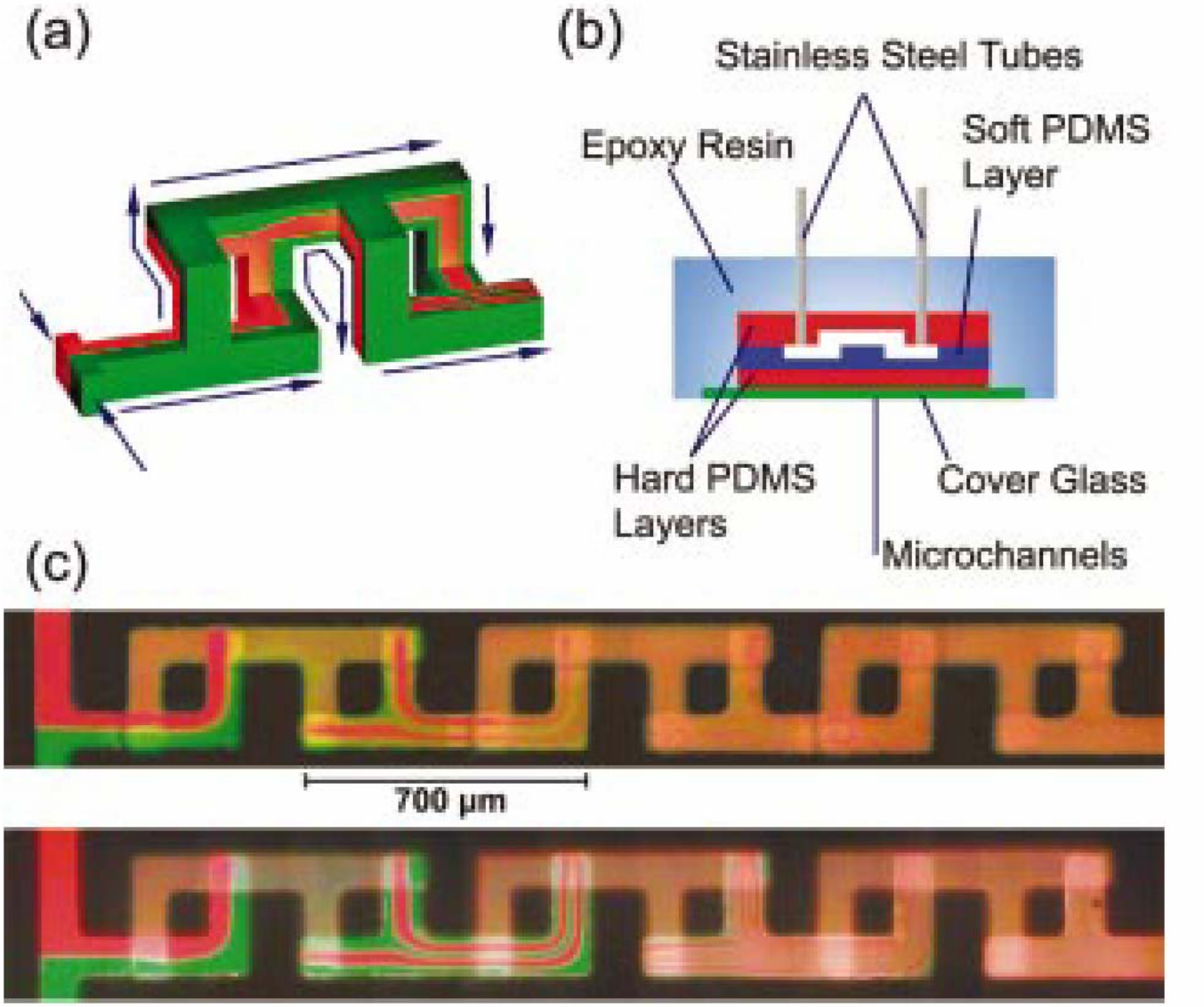

$100\,\mu m \times 70\,\mu m$ Channel cross-section

$400\,\mu m \times 300\,\mu m$ Stage of mixer

FIG. 1. (Color) (a) Topologic structure for microfluidic mixing. Two different solutions are combined in a T-junction. The fluid flow is repeatedly split, rotated, and recombined as indicated by the arrows. (b) Schematic cross-section of an assembled mixing chip. The two principal elastomer layers are fused together and anchored with a third elastomer layer on a glass cover slip. The chip is embedded in a block of epoxy resin for additional mechanical stability; steel tubes provide the inlets and outlet. (c) Mixing of two fluorescently labeled protein solutions in a six-stage mixer at a flow rate of 1 mm/s, corresponding to a Reynolds number of 0.1. (top). Mixing of the same dyes in an aqueous 54% glycerol solution with ten-fold higher viscosity at a flow rate of 10 mm/s, maintaining the same Reynolds number of 0.1 (bottom).

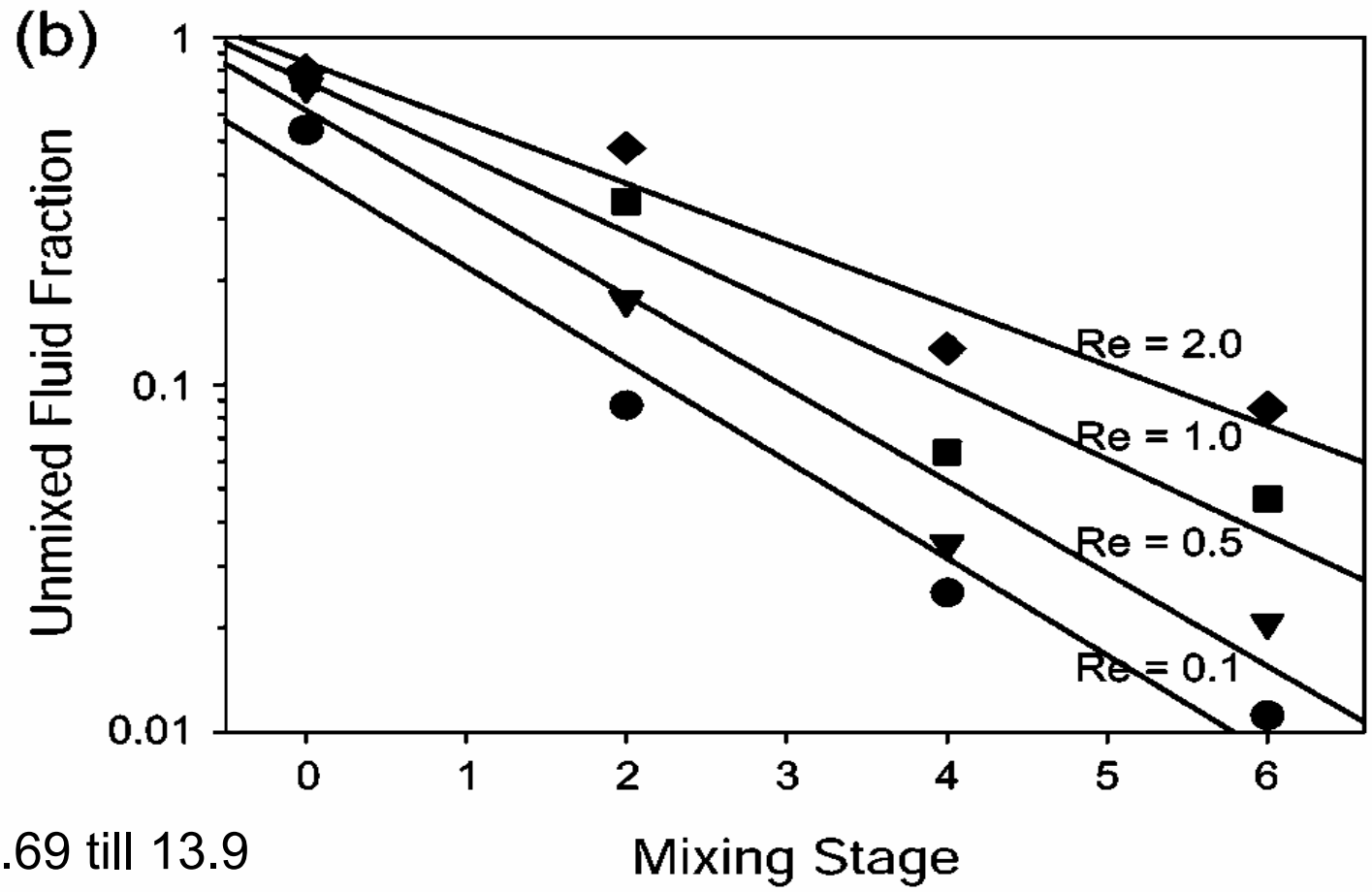

Pe from 0.69 till 13.9

FIG. 2. (a) Fluorescence across the flow channel after two mixing stages when a Ca^{2+}-sensitive dye is mixed with a $CaCl_2$ solution at different flow velocities, after the background is subtracted. The fluorescence of a pre-mixed solution is shown for comparison. (b) Fraction of unmixed fluid at each stage of the mixer for different flow rates, as determined from the fluorescence measurements. Linear regression lines in the semilogarithmic display indicate the exponential increase in mixing efficiency with channel length.

Chaotic mixing in a steady flow in micro-channel

C. Simonnet and A. Groisman, PRL **94**, 13401 (2005)

Flow can be chaotic not only in time-periodic flows but even in steady open flows, if flow lines are diverging exponentially.

As an example of such flow was considered in SHM mixer but it was not clear whether the decay was exponential as was found in the Batchelor regime mixer.

$180\,\mu m \times 50\,\mu m$

$\& \; 50\,\mu m \times 50\,\mu m$

$180\,\mu m \times 500\,\mu m$

Measuring segment

1.5mm or 0.8 mm
Stirring segment

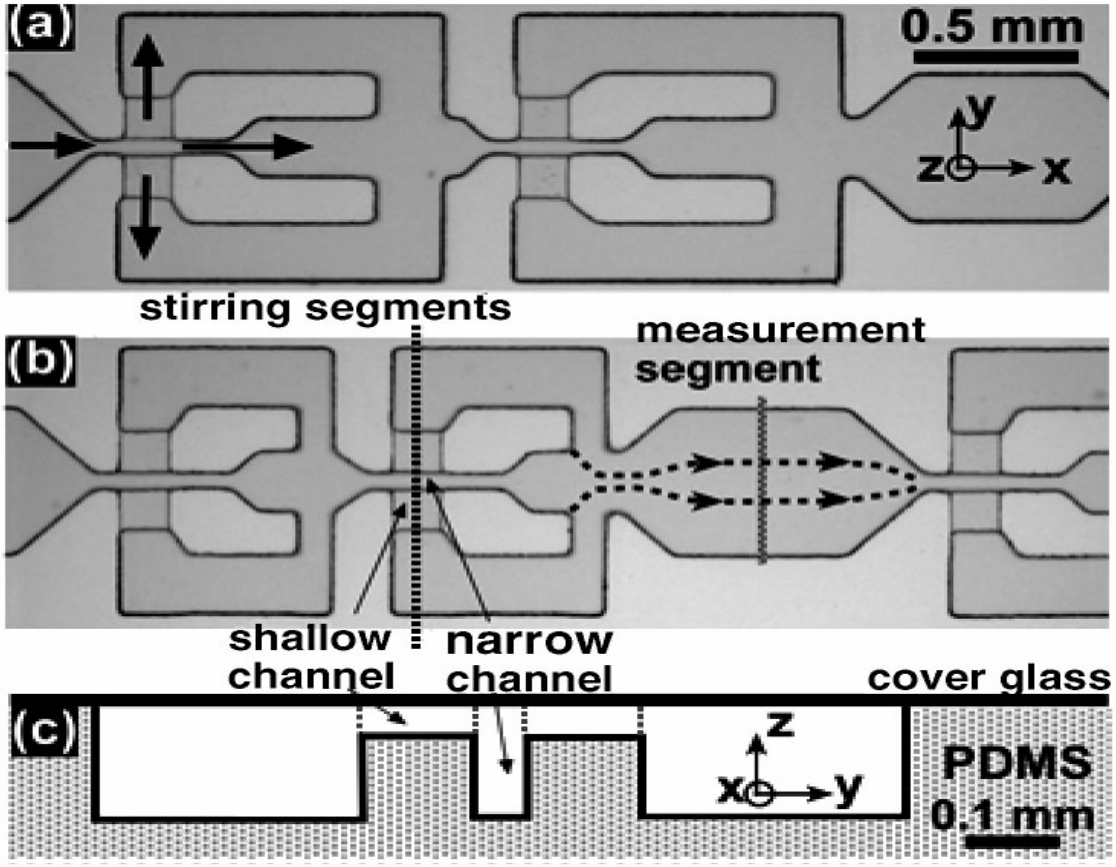

FIG. 1. (a),(b) Micrographs of fragments of the two mixer channels used in the experiments and (c) a schematic drawing of a cross section of a channel. The arrows in (a) show flow directions. The vertical dashed line in (b) indicates the site of the cross section in (c). The hatched area in (b) indicates the region where the confocal microscopy is made. The two dashed lines with arrows in (b) show the lines of merging between the streams from the stirring segment. **34 stirring elements**

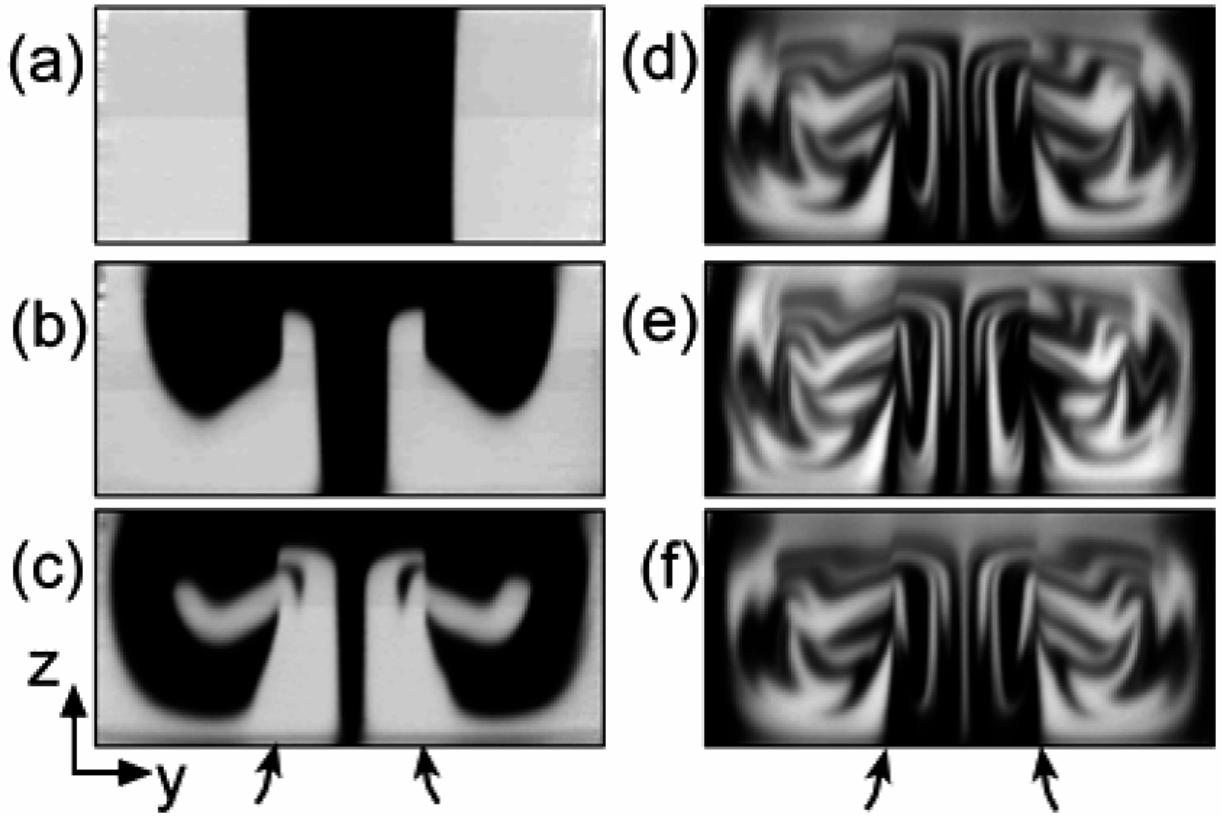

FIG. 2. Confocal micrographs showing distributions of the fluorescent dye over the cross sections of the measurement segments: (a) before the entrance ($N = 0$); (b), (c) and (d)–(f) at $N = 1$, 2, and 6, respectively. Micrographs (d)–(f) correspond to three different copies of the same mixer. The curved arrows at the bottom mark the boundaries between the streams from the stirring segment [cf. Fig. 1(b)].

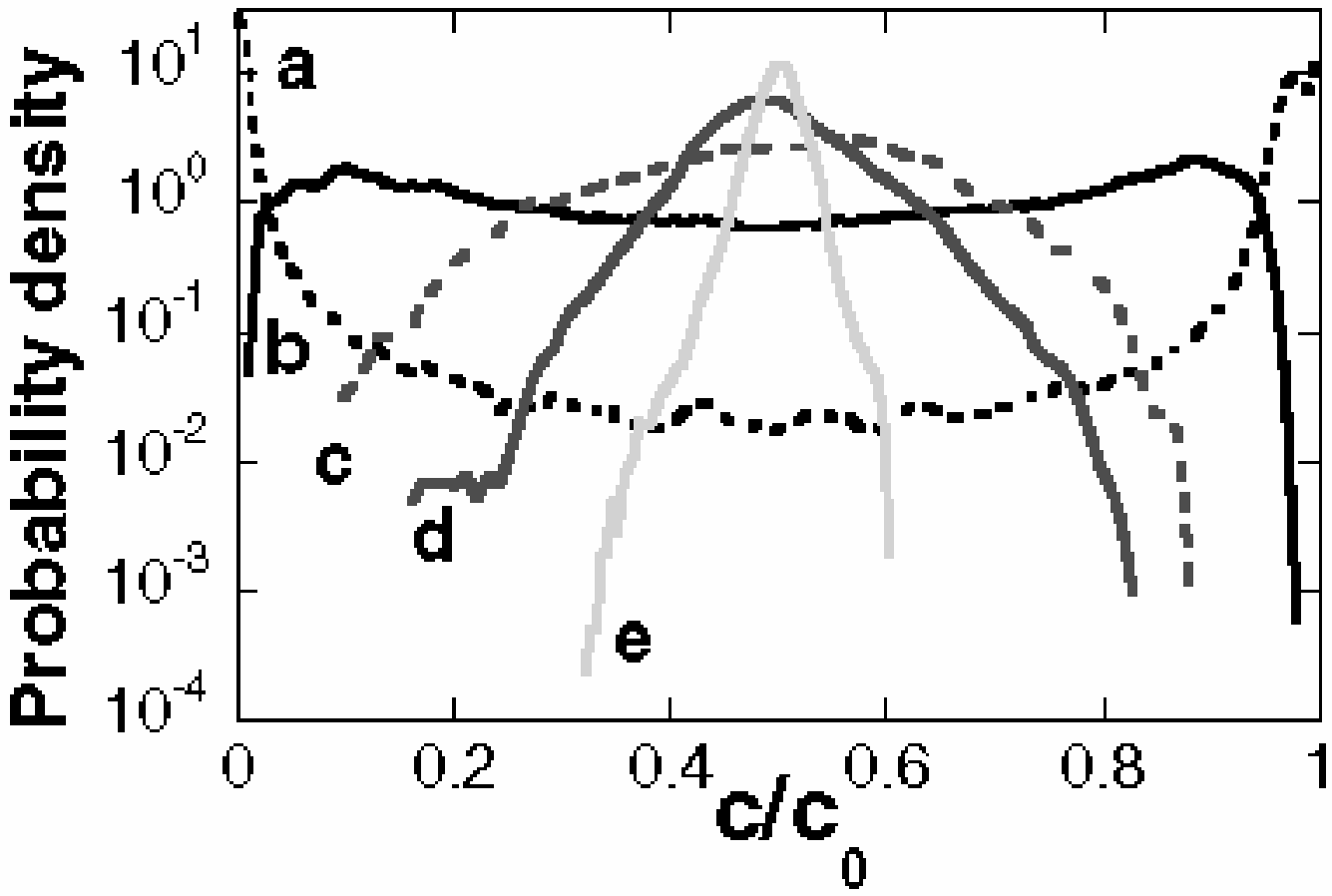

FIG. 3. Plots of PDF of the concentration of the fluorescent dye at $\mathrm{Pe} = 2.6 \times 10^5$ and different positions. Curves a, b, c, d, and e correspond to $N = 0$, 4, 10, 14, and 22, respectively.

$$M_i \propto \exp[-\gamma_i(Pe)N]$$

$$N_{mix} = 1/\gamma_1; N_{mix} \propto Pe^{\alpha}$$

$$L_{mix} = N_{mix} L_s$$

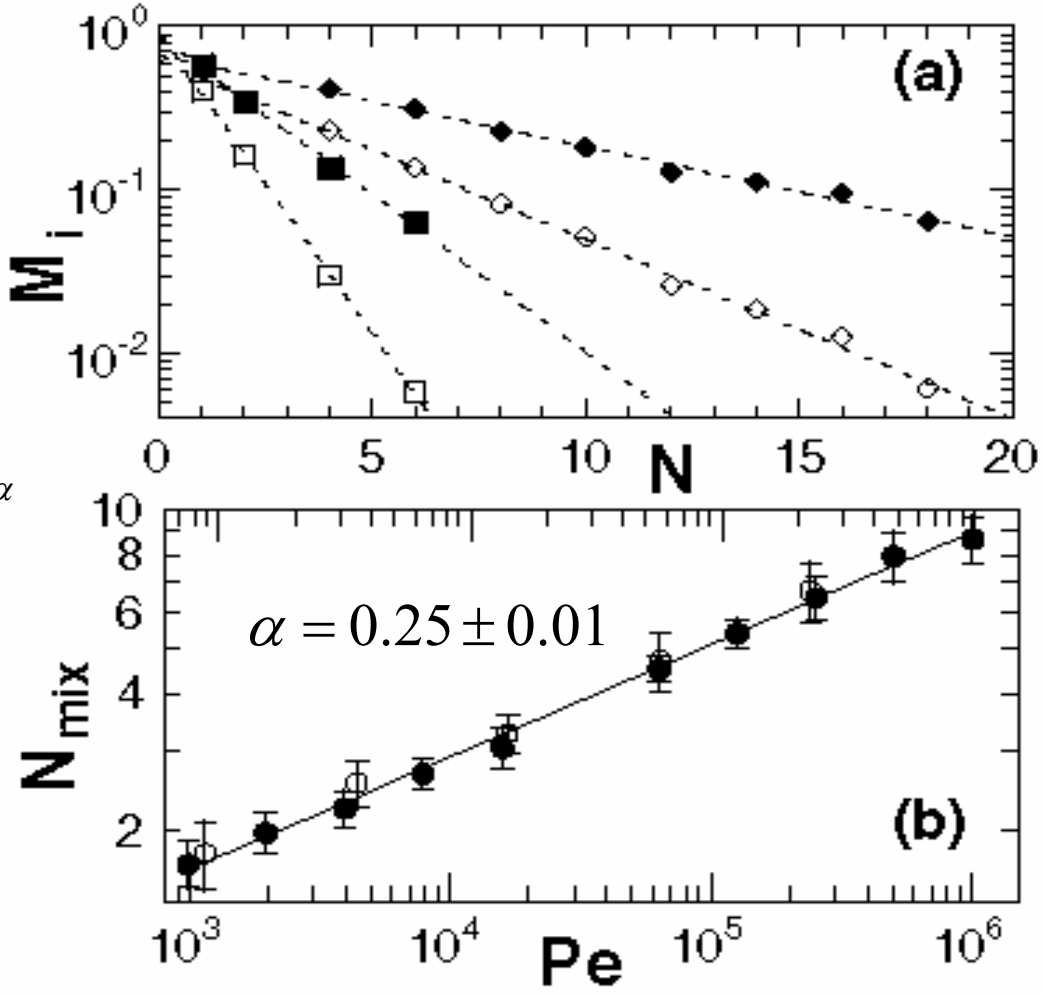

FIG. 4. (a) The moments M_1 (solid symbols) and M_2 (open symbols) of PDF of the dye concentration as functions of N at $\mathrm{Pe} = 4.0 \times 10^3$ (squares) and $\mathrm{Pe} = 2.6 \times 10^5$ (diamonds). (b) The mixing length, N_{mix}, as a function of Pe for the mixers in Figs. 1(a) and 1(b), solid and open symbols, respectively. The solid line is a power law fit.

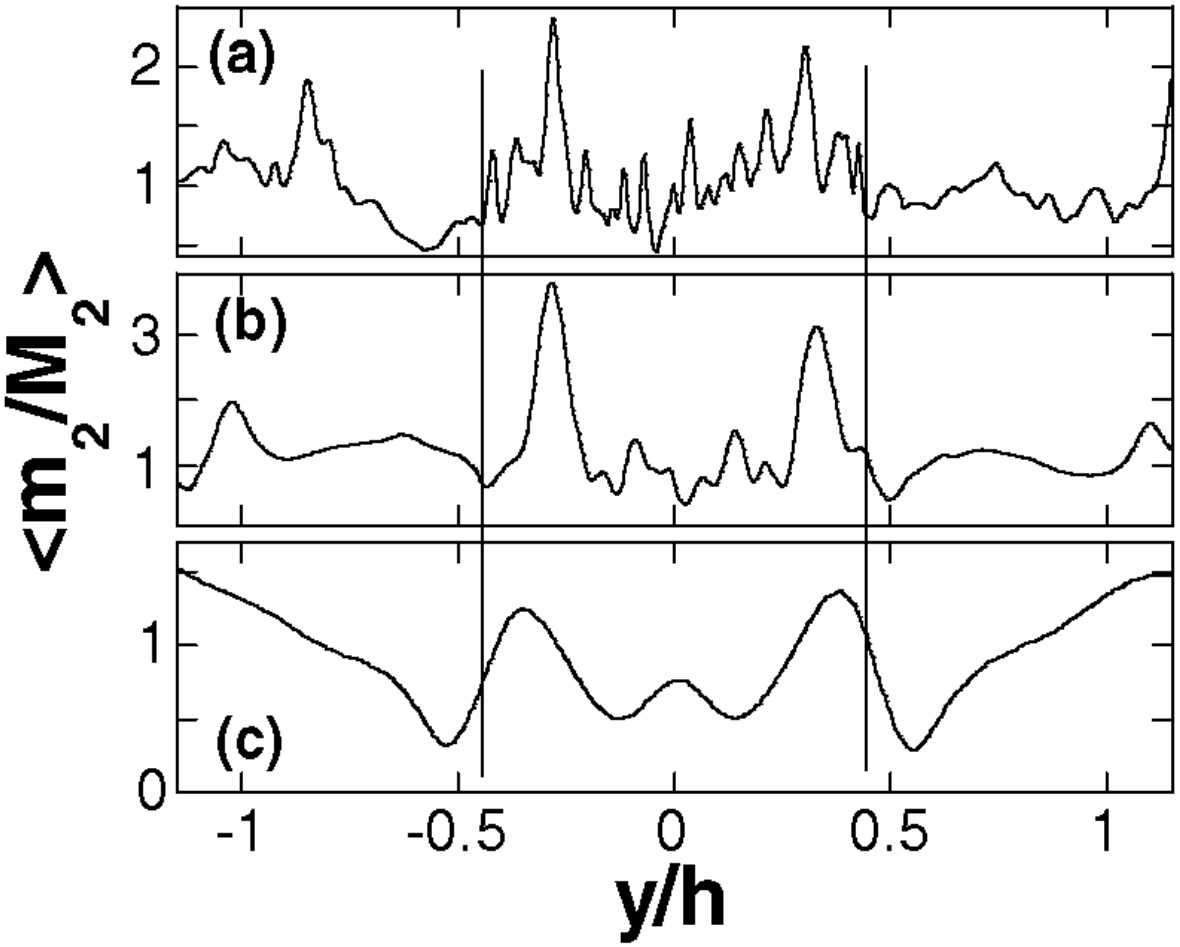

FIG. 5. Spatial dependence of $\langle m_2(y)/M_2 \rangle$ on the position, y, across the microchannel measured from the center: (a) Pe $= 1.0 \times 10^6$, (b) Pe $= 2.6 \times 10^5$, and (c) Pe $= 1.0 \times 10^3$. The vertical lines show the locations of the boundaries between the three merging streams [cf. Figs. 1(b) and 2].

Spatio-temporal resonances in mixing of open viscous fluids

F.Okkels&P.Tabeling, PRL **92**, 038301(2004)

An attempt to produce an interface instability via external driving-new dynamical phenomenon that can occur in a broad range of viscous, periodically driven open system- example of active mixer

Re<1, creeping flow, linear mixer

$$d\vec{X}/dt = \vec{V}_M + f(t)\cdot\vec{V}_T,$$

$$\alpha = \frac{A}{V}; \Omega = \omega\frac{L}{V}; f(t) = \alpha\cos\Omega t$$

$\vec{V}_M(\vec{V}_T)$ are the main (transverse) velocity flows

***V*-main velocity**

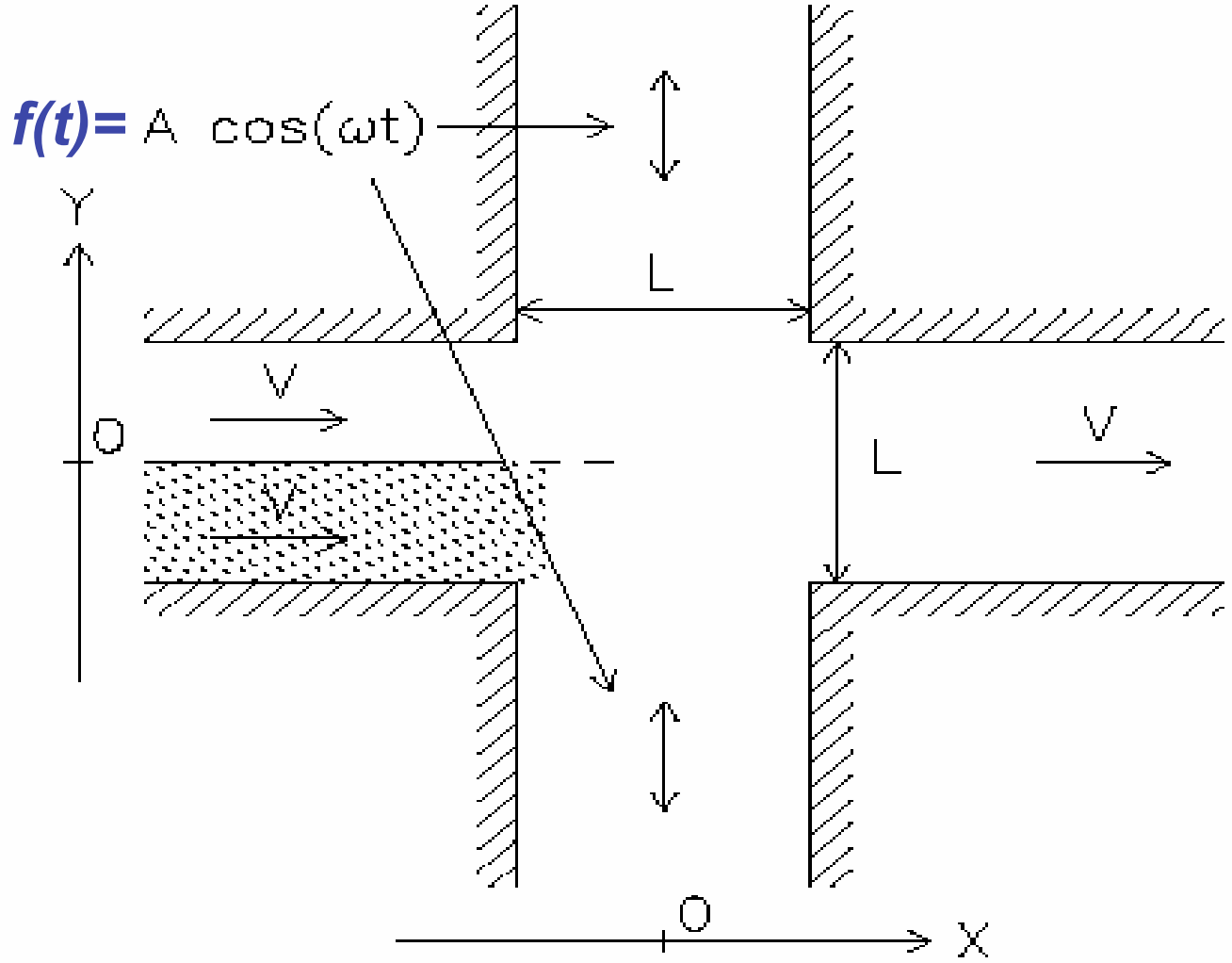

FIG. 1. Schematic setup of the mixer with the characteristic quantities and axes.

$\Omega > \alpha$

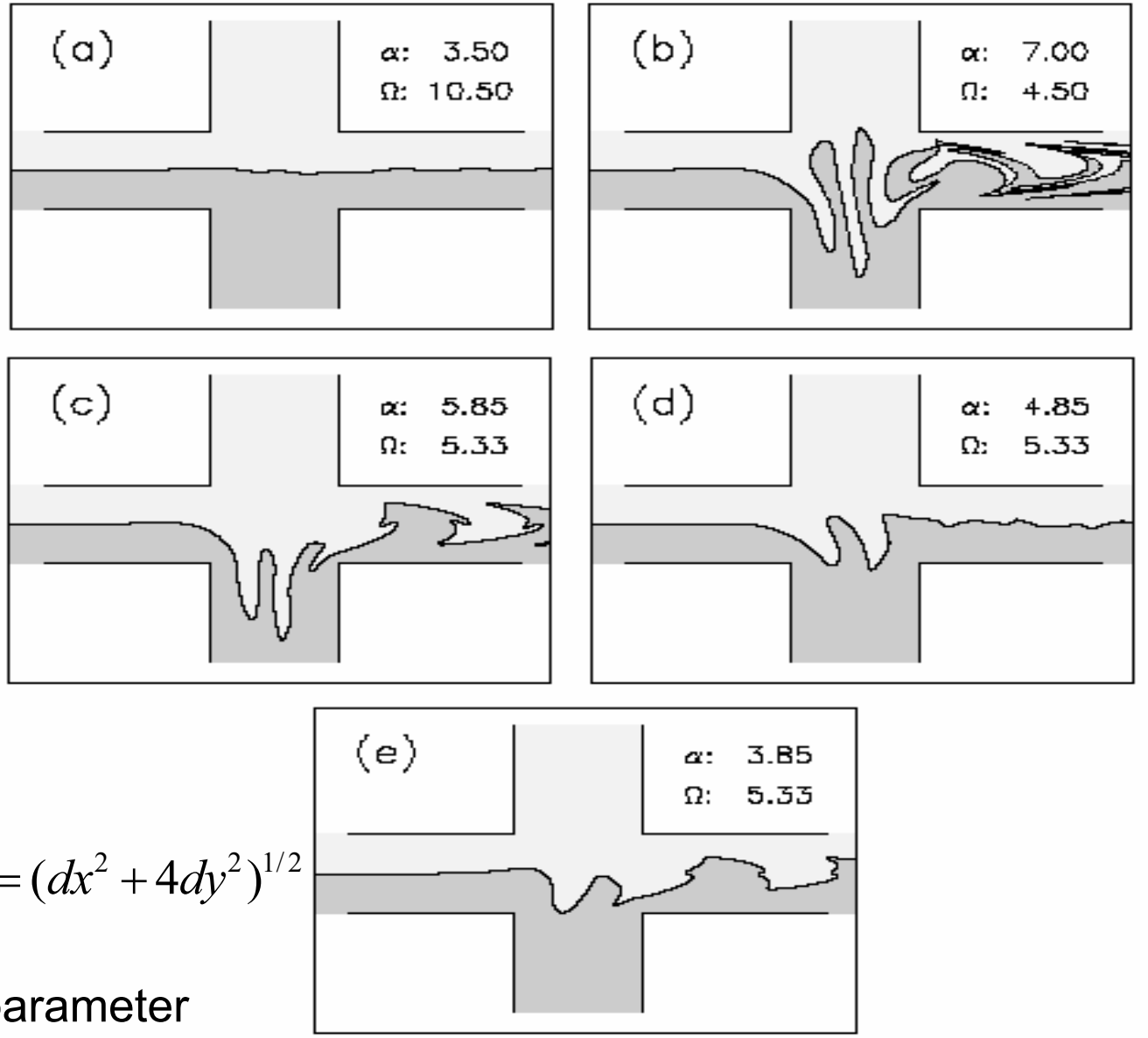

$\Omega < \alpha$

$$F = \frac{L_a}{L_r} - 1; L_r = (dx^2 + 4dy^2)^{1/2}$$

F-folding parameter

FIG. 2. Example of interface snapshots for different control parameters: (a)/(b), poor/strong mixing; (c)–(e), strong local variations in mixing efficiency.

$$T_A = C_n T_P;$$
$$C_n = n + 1/2;$$
$$T_P = 2\pi / \Omega$$

T_a -advection time

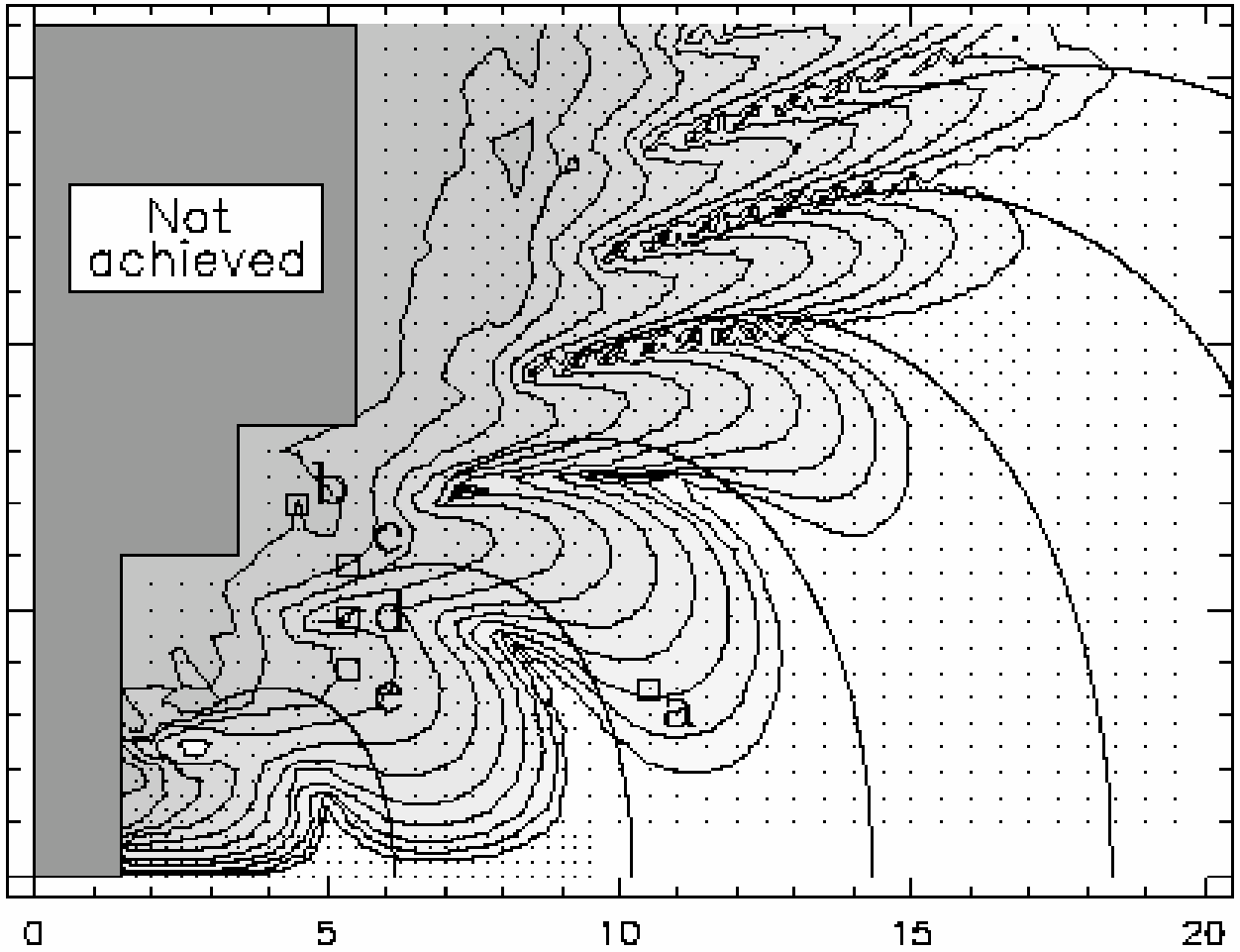

$$10^{-3} \le F \le \approx 4.64$$

Gray scale is proportional to logF

FIG. 4. Contour plot of the folding quantity F as a function of the control parameters Ω, α. Points for each measurement of F; squares for states shown in Fig. 2; solid curves for theoretical resonances predicted by Eq. (9). (good mixing-dark)

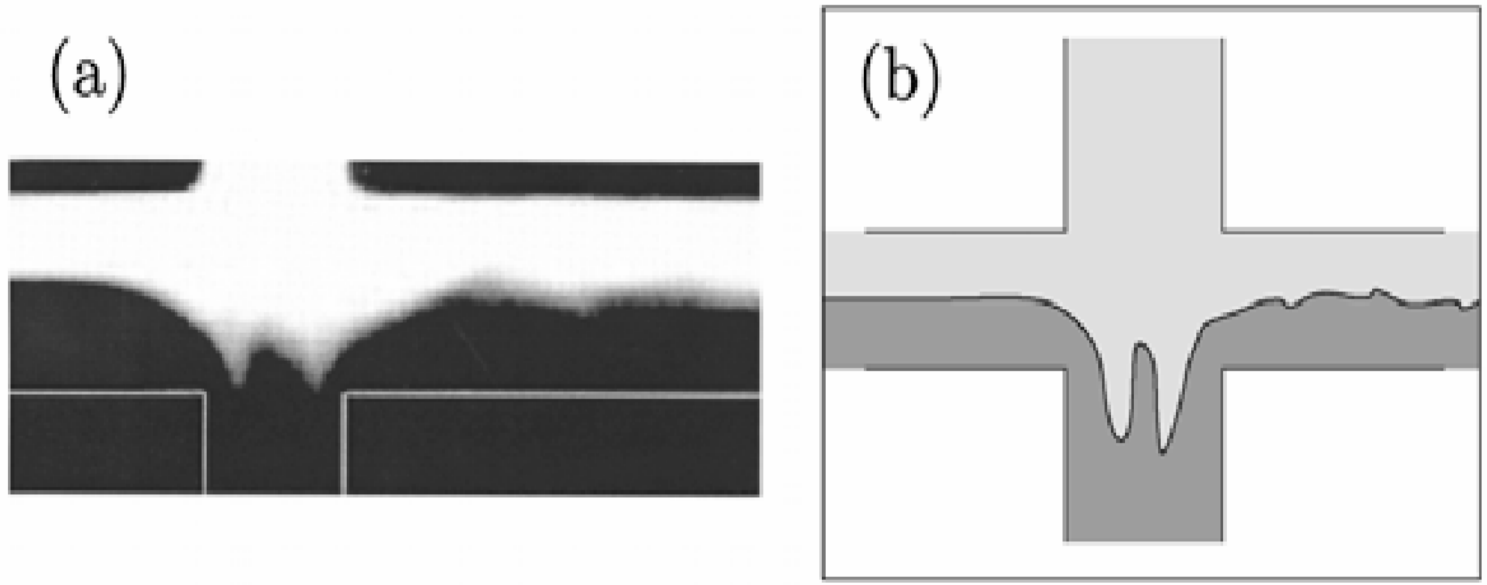

FIG. 5. Indication of an experimental second resonance state (a) compared to similar numerical state (b).

Hydrodynamic focusing: mixing nanoliters in microseconds

J. Knight et al, PRL **80**, 3863 (1998)

$\alpha = P_s / P_i$ Focusing is observed in some range of α

$$\alpha_{\min} = 0.48 \pm 0.01 \,\&\, \alpha_{\max} = 1.28 \pm 0.01$$

Focusing can be described by a simple circuit model:

$$P, Q \Rightarrow U, I$$

Relation between fluid flux and pressure is the same as Ohm's law due to linear equations of motion for low Re viscous fluid

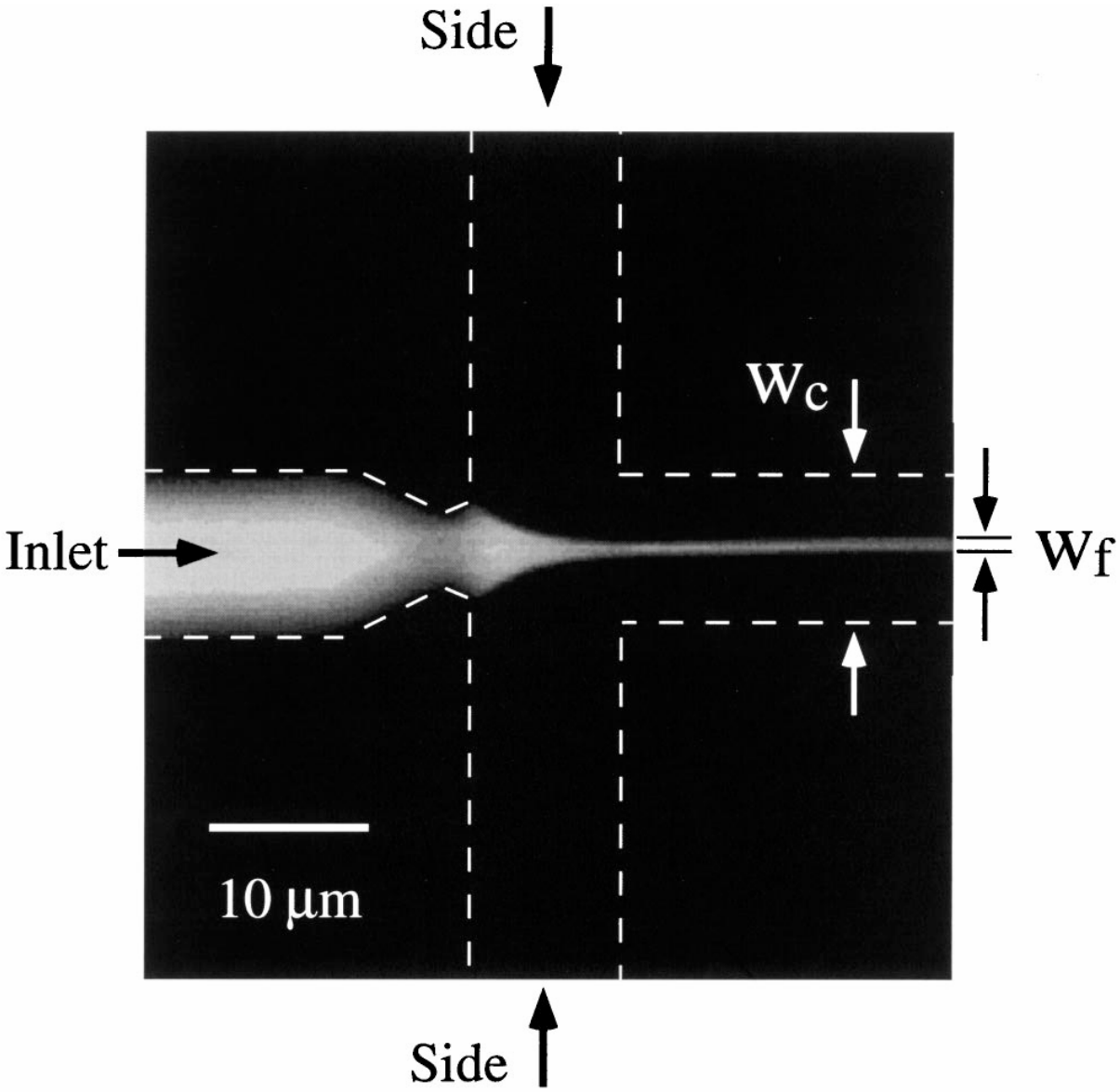

FIG. 1. Hydrodynamic focusing with $P_i = 5$ psi and $\alpha = 1.1$. The edges of the channels are outlined with a dashed line for reference. The variables w_c and w_f describe the width of the channel (10 μm) and the width of the focused inlet stream.

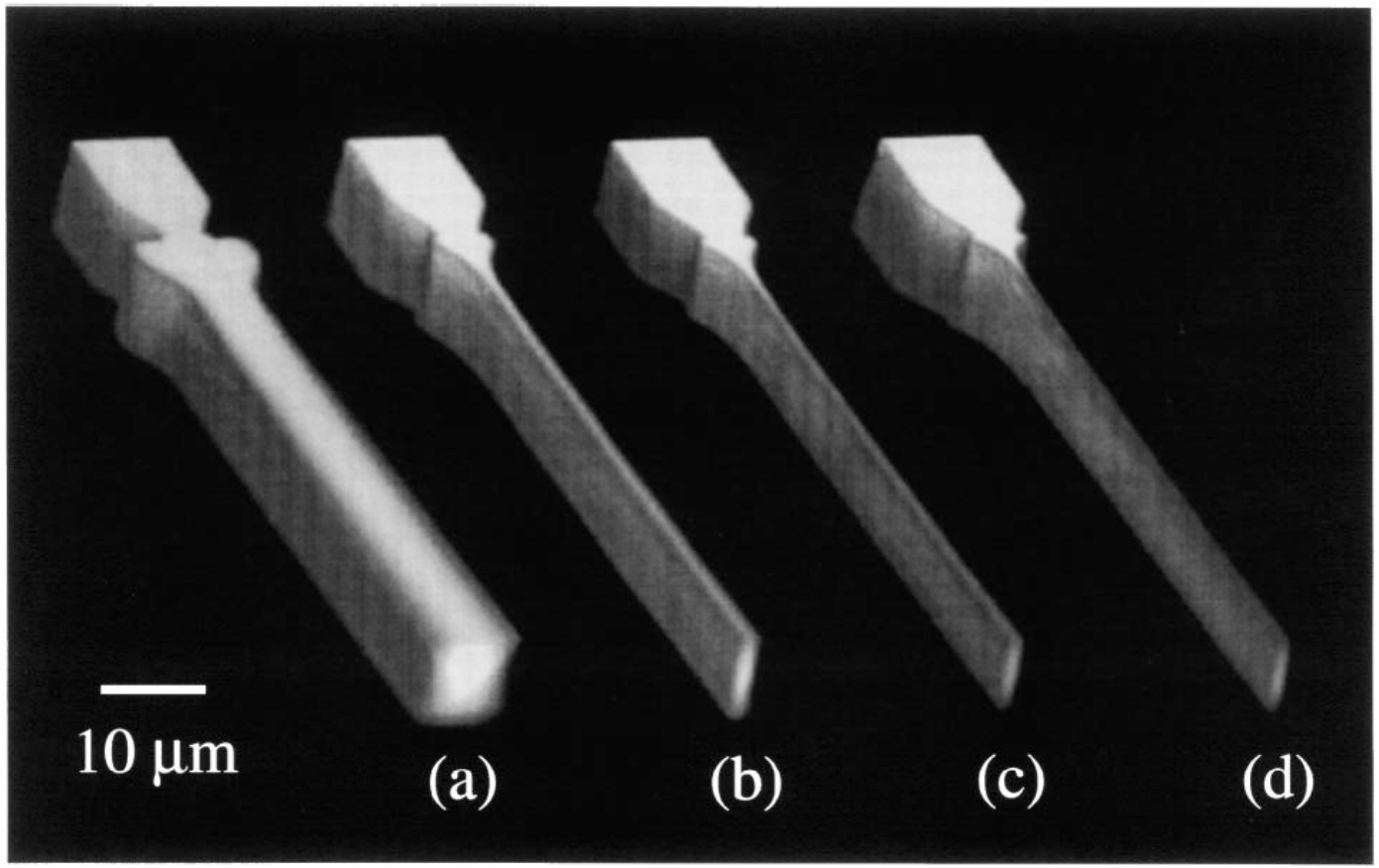

FIG. 2. Confocal scanning microscopy images of hydrodynamic focusing with $P_i = 5$ psi and (a) $\alpha = 0.5$, (b) 1.0, (c) 1.1, and (d) 1.2. Fluorescein was used to label the inlet flow and appears bright. Each three-dimensional rendering is formed from approximately 30 separate two-dimensional images acquired at regular intervals in depth.

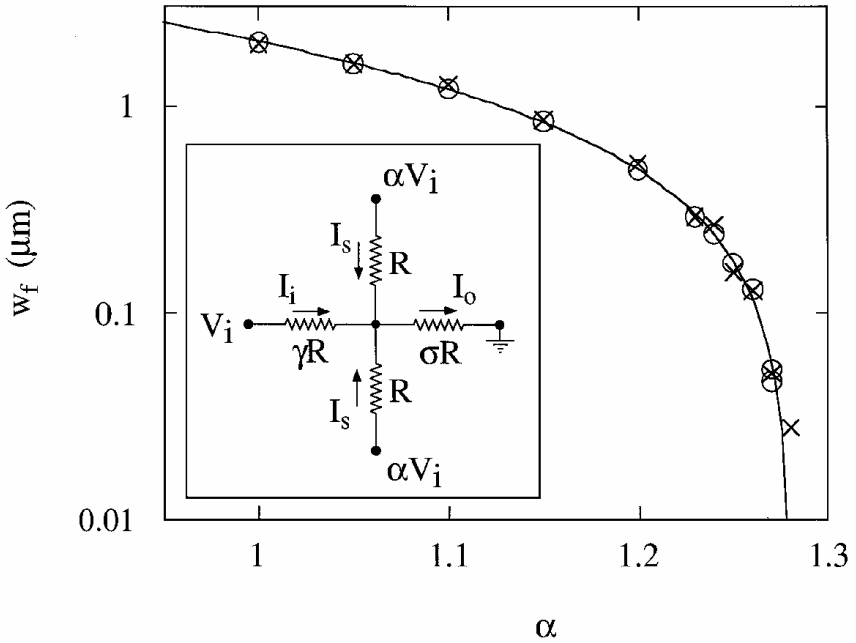

FIG. 3. The width of the focused inlet stream plotted on a logarithmic scale against α. The inlet pressure was held constant at $P_i = 10$ psi. Data from two separate experiments (× and ○) are shown and agree within experimental error. The solid line is a one parameter, least-squares fit to Eq. (2) with $B = 1.6$. The inset is a diagram of the resistive circuit corresponding to fluid flow in the mixer.

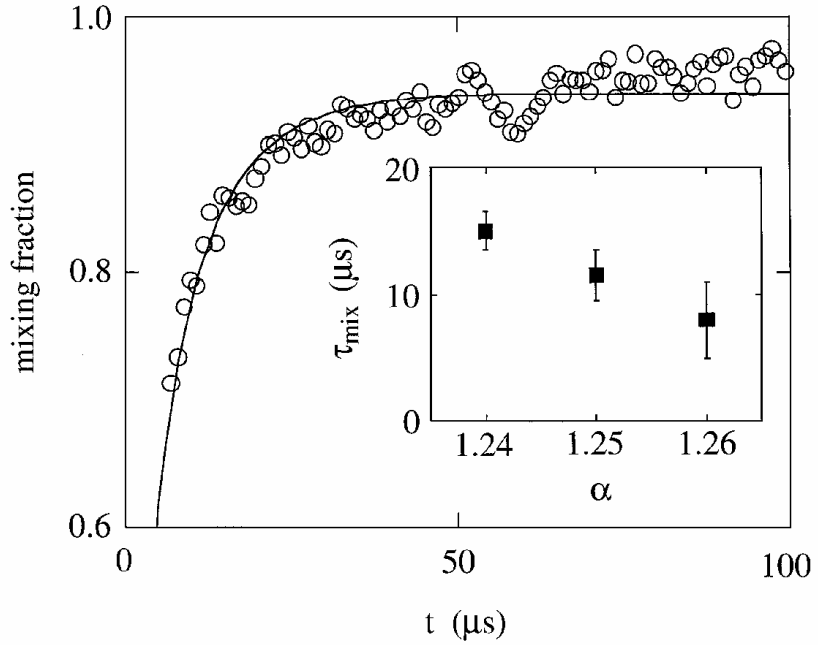

FIG. 4. The mixing fraction as a function of time for $P_i = 40$ psi and $\alpha = 1.25$. Reaction time t was calculated by dividing the distance along the focused stream from the point of initial focus by the flow velocity. The solid line is a best fit to a functional form calculated for diffusion into a rectangular cross section. The inset shows the mix times determined from similar fits to mixing data obtained for several values of P_i and α.

$$\frac{w_f}{w_c} = B\frac{(1+2\sigma-2\sigma\alpha)}{(1+2\sigma\gamma\alpha)}$$

focusing ratio

γ ratio of the inlet resistance to the side resistance